

Improvements in Fiber Optic Coupler Fabrication Techniques

by

Veerendra B. Vuppala

Thesis submitted to the faculty of the

Virginia Polytechnic Institute and State University

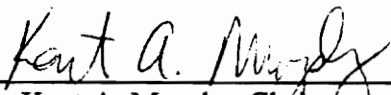
in partial fulfillment of the requirements for the degree of


MASTER OF SCIENCE

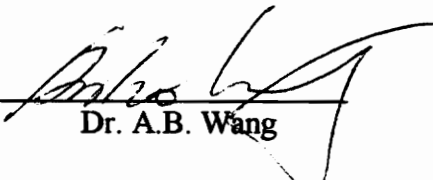
in

Electrical Engineering

Approved:


Dr. Kent A. Murphy, Chairman


Dr. Ira Jacobs


Dr. A.B. Wang

September 1994,

Blacksburg, Virginia

c.2

LD
5655
V855
1994
V877
c.2

Improvements in Fiber Optic Coupler Fabrication Techniques

by

Veeru B. Vuppala

Dr. Kent A. Murphy, Chairman

Electrical Engineering

(Abstract)

A novel coupler measurement station and technique for manufacturing fused biconical tapered multi-port multimode couplers with improved uniformity among ports is presented. Improvement in the uniformity of the couplers is achieved by diffusion of the minimum taper region of the coupler. The phenomenon of dopant transport from the core to the cladding (or from the cladding to the core) at high temperatures is known as diffusion. Diffusion of a germanium-doped core results in the germanium dopants migrating from the core into the cladding thus increasing the effective diameter of the core which is accompanied by a decrease in the refractive index. The cores of individual fibers in the minimum taper region are a few micrometers apart. Diffusion thus results in a minimum taper region that has approximately uniform refractive index leading to better uniformity among ports.

The experimental setup and results of diffusion tests on multimode fiber with different core/cladding ratios are presented. A coupler station that is capable of making bi-

directional measurements of the coupler is demonstrated successfully. The coupler station also enables a user to dynamically monitor the ports of the coupler during manufacture, and can be adapted to manufacture star couplers ranging in size from two to sixteen fibers.

Acknowledgements

I would like to express my gratitude to Dr. Kent Murphy for serving as my advisor, and committee chair. I would also like to thank the members of my committee, Dr. Ira Jacobs and Dr. A.B. Wang.

I would like to thank Dr. R.O.Claus for continued support during my graduate life. I would also like to acknowledge Mallika Sen, Mike Gunther, and Nirmal for their invaluable support and help during the course of my thesis. I also thank the staff and students of FEORC for their support.

A sincere thanks to my parents and my brother without whose help I would never have been able to make it this far. This acknowledgement would not be complete without mention of my late grandmother who encouraged and guided me. I would also like to thank my very special friend Soumya for being there. A very special thanks to all my friends who made my stay at Virginia Tech enjoyable.

Table of Contents

| | |
|---|-----|
| Acknowledgements | iv |
| Table of Contents | v |
| List of Illustrations | vii |
| List of Tables..... | x |
| 1.0 Introduction..... | 1 |
| 1.1 Couplers | 4 |
| 1.1.1 Three-Port Couplers..... | 4 |
| 1.1.2 Star Couplers..... | 5 |
| 1.1.3 Wavelength Division Multiplexing Couplers..... | 8 |
| 1.1.4 Integrated Optic Couplers..... | 8 |
| 1.2 Fused Biconical Tapered Couplers | 9 |
| 1.3 Coupler Parameters..... | 11 |
| 1.4 Uniformity improvement techniques | 12 |
| 2.0 Theory..... | 18 |
| 2.1 Ray Analysis of Multimode Fibers | 22 |
| 2.2 Variations in Bound Power with Normalized Frequency | 32 |
| 3.0 Diffusion..... | 36 |
| 4.0 Coupler Station | 45 |
| 4.1 Source/Detector Array | 46 |
| 4.1.1 The Light Emitting Diode (LED) Lens Alignment..... | 46 |
| 4.1.2 Fiber Lens Alignment..... | 49 |
| 4.1.3 Detectors..... | 51 |
| 4.2 Coupler Tapering Stage..... | 58 |

| | |
|--|----|
| 4.3 Software | 58 |
| 5.0 Results..... | 66 |
| 5.1 Push-Pull Technique..... | 66 |
| 5.2 Diffusion Technique..... | 67 |
| 5.2.1 Results of 100/140 Multimode Fiber Couplers | 67 |
| 5.2.2 Results of 62.5/125 Multimode Fiber Couplers | 73 |
| 6.0 Conclusions | 85 |
| 7.0 References | 88 |
| Vita..... | 93 |

List of Illustrations

| | |
|--|----|
| Figure 1a. Three port coupler manufactured by offset method..... | 6 |
| Figure 1b. Three port coupler made by the semi-transparent method..... | 6 |
| Figure 1c. Three port coupler made by the fused biconical taper method..... | 6 |
| Figure 2a. Diffraction grating coupler with grating on a graded lens..... | 10 |
| Figure 2b. A fused biconical tapered coupler..... | 10 |
| Figure 3. Push-pull method for improvement of uniformity | 15 |
| Figure 4. The s-Bend method for improvement of uniformity of couplers..... | 16 |
| Figure 5. The mixer rod method for uniformity improvement. | 17 |
| Figure 6a. Refractive index profile of step-index fiber. | 20 |
| Figure 6b. Refractive index profile of graded-index fiber..... | 20 |
| Figure 7. Variation of refractive index profile of the fiber for various ' α ' profiles (from G. Keiser [15])..... | 21 |
| Figure 8. Ray components in a graded-index fiber..... | 25 |
| Figure 9. Cross sectional projection of a ray in a graded-index fiber..... | 29 |
| Figure 10. Plot of l/v and N/V | 30 |
| Figure 11. Propagation constant of the modes as a function normalized frequency. | 31 |
| Figure 12. Power flow in the core versus the normalized frequency number..... | 35 |
| Figure 13. Variation in refractive index as a function of doping concentration in silica glass..... | 38 |

| | |
|--|----|
| Figure 14. Refractive index profile of silica core fiber. Unheated (1), heated at $\sim 1950^{\circ}$ C for 6s (2), for 25s (3), and for 40s (4). | 42 |
| Figure 15. Measured GeO_2 concentration as the function of radial distance from the center of the fiber. | 43 |
| Figure 16. Refractive index change as a function of taper length..... | 44 |
| Figure 17. Block diagram of coupler station..... | 47 |
| Figure 18. LED/lens assembly in a brass barrel..... | 50 |
| Figure 19. Fiber-lens assembly in a brass barrel. | 52 |
| Figure 20. Circuit of the trans-impedance amplifier used for detectors..... | 53 |
| Figure 21. Plot of output voltage of the trans-impedance amplifier versus the incident optical power for the throughput detector..... | 55 |
| Figure 22. Plot of output voltage of opamp and incident optical power with LED drive current for reference detector..... | 56 |
| Figure 23. The source/detector system with the LED/lens barrel and the fiber/lens barrel..... | 57 |
| Figure 24. Experimental setup for measuring modal power distribution of the fibers..... | 59 |
| Figure 25. Plot of modal power distribution for unit #6..... | 60 |
| Figure 26. Coupler tapering stage. | 61 |
| Figure 27. Transmission matrix produced by the software. | 65 |
| Figure 28. Push-pull method. | 68 |
| Figure 29. The comparison of tradeoff between excess loss and uniformity with time. | 77 |

Figure 30. Uniformity versus time at various temperatures. 78

Figure 31. Excess loss versus time at various temperatures. 79

Figure 32. Modal power distribution of throughput fiber before fusion. 82

Figure 33. Modal power distribution of throughput fiber after diffusion. 83

Figure 34. Modal power distribution of tapoff fiber after diffusion. 84

List of Tables

| | |
|---|----|
| Table I. Transmission matrix of the coupler before uniformity improvement..... | 69 |
| Table II. Transmission matrix of the coupler after push-pull technique is applied..... | 70 |
| Table III. Transmission matrix of the coupler before uniformity improvement. | 71 |
| Table IV. Transmission matrix of the coupler after diffusion technique is applied. | 74 |
| Table V. Improvement in uniformity of the coupler with time..... | 75 |
| Table VI. Results of diffusion tests on 8x8 couplers..... | 76 |
| Table VII. Transmission matrix of the coupler with a taper length of 0.8 cm during diffusion. | 80 |
| Table VIII. Transmission matrix of coupler with a taper length of 0.5 cm during diffusion | 81 |

1.0 Introduction

The need for transporting diverse information over local area networks (LANs) has fueled the rapid development of high bandwidth technologies and as a result optical fibers are being increasingly used in communication systems. The development of low cost, low loss optical fiber has led to the use of fiber optic systems as the preferred medium of communication systems. Optical fiber has a greater information carrying capacity over longer distances at costs lower than the conventional copper wire transmission systems. Optical fibers are also used in point to point communication systems in addition to local area networks with complex topologies such as star, ring, bus etc.

Optical fiber LAN's are being accepted as the technology for optical point-to-point data transmission [1-4]. Optical fibers are also being installed in long-haul, short-haul communication systems, broadcast networks etc.. Future broadband integrated service digital network (B-ISDN) systems require interconnection of the existing fiber optic local area networks [5]. Interconnection of these networks can be achieved by two means either active or passive interconnection. A passive interconnection is one in which light is split or combined without being converted into the electrical domain and is achieved through devices such as star couplers, T coupler, and other coupler devices. Passive interconnection of networks is more desirable compared to active interconnection because it is superior in reliability and lower in cost [6].

Often for LAN applications, the signal must be split to several subscribers, or signals from several lines have to be combined onto a single main line, or the fiber has to be used as a bi-directional transmission medium. These operations can be performed on the optical signal without conversion of the optical signal to electrical signal, by passive optical devices such as optical couplers. Applications such as splitting or combining optical signals, linking several transmitters and receivers together or bi-directional transmission of information over one fiber, use fiber optic couplers.

Fiber optic star couplers are an essential component in various network topologies where a signal has to be divided among several subscribers within a loop. An ideal star coupler is one in which the signal on a particular arm is distributed equally among all ports. There

are several methods for manufacturing star couplers but the most widely used technique for manufacturing star couplers is the Fused Biconical Tapered (FBT) technique. FBT has emerged as the most reliable and convenient technique for manufacture of couplers because it is suitable for mass production of environmentally stable couplers. Moreover FBT coupler manufacturing technique can be adapted to suite a wide range of applications and specifications relatively easily. The most important drawback of these multimode FBT couplers is that the port-to-port variations are very large because of the modal dependency of the manufacturing technique. Distributed optical uniformity is important for star couplers to enable the use of narrow dynamic range receivers which are generally less expensive than wide dynamic range receivers.

The objective of this thesis is to develop less complex methods for manufacture of low loss, high uniformity fiber optic couplers. Results are obtained from couplers manufactured on a coupler station developed as a part of this thesis. Chapter 2 briefly describes the theory of multimode fibers and the variation of bound power in the core of the fiber with changes in radius. Chapter 3 discusses the diffusion phenomenon in fibers. Chapter 4 includes details of the coupler station developed to conduct diffusion tests on multimode multiport couplers. The results of the diffusion tests are presented in Chapter 5. Conclusions and future work are discussed in Chapter 6.

1.1 Couplers

Fiber optic coupler is a passive multiport device that combines or distributes optical power. Couplers are used extensively in optical fiber based communication systems. Fiber optic couplers can be divided into four groups according to their characteristics [7].

- Three-Port Couplers
- Star Couplers
- Wavelength Division Multiplexers(WDMs)
- Integrated optic couplers

1.1.1 Three-Port Couplers

Three port couplers or 'Y' couplers are couplers in which light from one port is split among two output ports. These couplers are also known as 'T' couplers if one arm of the coupler splits only a small amount of light. These couplers are used for bus networks in optical LAN systems to split the signal to individual nodes. Three port couplers are manufactured by several different methods. The offset method, shown in Figure 1a, uses an "overlapping" of the endfaces. The light from the input waveguide is distributed into the output waveguide depending on the degree of overlap of the fibers. Couplers manufactured by this method incorporate step-index fibers and have a high excess loss because all light in the outgoing fiber is not coupled into the other fibers. Bi-directional couplers can be fabricated using this method. The semi-transparent-mirror method, shown

in Figure 1b, incorporates an angled surface, which is partially reflective placed in the propagation path of the main fiber. The reflected light is collected by the other arm of the three port coupler. Optical power in the input port is coupled into the output port . The amount of power coupled into either of the ports depends on the thickness of the semi-transparent mirror.

Another method of manufacturing the three port couplers is by the Fused Biconical Taper (FBT) technique. Two fibers are twisted and then heated in the middle until they fuse together as shown in Figure 1c. The FBT method is the most common method of manufacturing couplers.

1.1.2 Star Couplers

Star couplers are used to divide the light from a single port to multiple ports. Star couplers that distribute optical signals simultaneously to many nodes, are required in optical data bus systems using duplex transmission. They are designed to be used in multiple access networks and broadcast applications. There are four types of manufacturing technologies for star couplers, mixer rod, etching, polishing and fused biconical taper approaches [8-11]. Mixer rod couplers use end-fire coupling while the etching, polishing, and fused biconical tapered couplers use mode coupling.

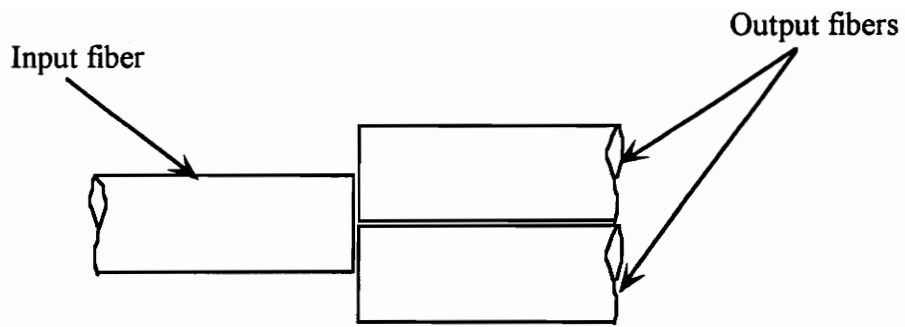


Figure 1a. Three port coupler manufactured by the offset method.

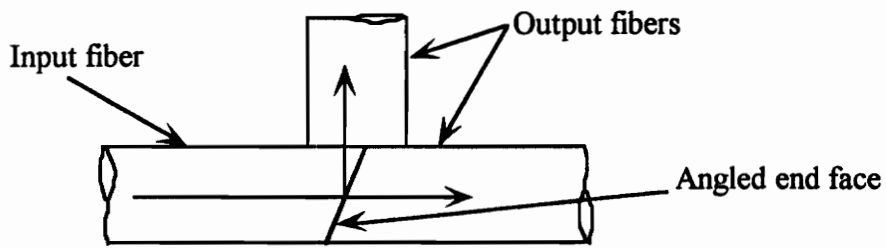


Figure 1b. Three port coupler made by the semi-transparent method.

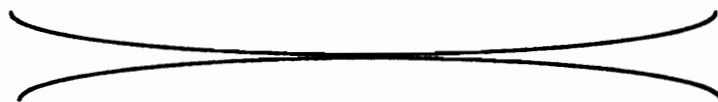


Figure 1c. Three port coupler made by fused biconical taper method.

A mixer rod star coupler uses multi-reflection technique to obtain power distribution among ports [12]. The mixer rod method has a thin mixer plate made of quartz glass to ensure that light coming out of any fiber is divided equally among all the output ports. The thickness of the mixer plate is equal to the thickness of the fiber and the width of the mixer plate is the sum of the dimensions of the fiber that makes up the coupler. Two types of couplers are made using this principle mixer rod, transmissive star and mixer rod reflective star.

Couplers are made by the etching approach by twisting the fibers that make up the coupler, and etching the cladding with hydrofluoric acid until the desired coupling takes place. In the polishing approach, cladding of the fibers is polished for a length of 2 mm until the desired coupling takes place. In the fused biconical tapered coupler process, the fibers are twisted, heated and pulled. The resultant fused section provides the coupling. The fused biconical tapered method relies upon the coupling of the higher order propagation modes into the other fibers and is thus highly mode dependent. This modal dependence results in high port-to-port variations when compared to couplers made by mixer rod principle.

1.1.3 Wavelength Division Multiplexing Couplers

Wavelength Division Multiplexing (WDM) couplers are used in wide band and integrated services transmission systems to improve transmission capacity of an optical fiber cable. These type of couplers are made by either diffraction gratings or dichroic filters [8]. The diffraction grating couplers have a grating on a graded index lens at the opposite end of a coupler as shown in Figure 2a. The light from the fiber is incident on the grating and each wavelength is reflected at a different angle. This light is coupled into particular fibers which are placed at appropriate angles to the grating. In the dichroic filter process the fibers are inserted in v-grooves in a glass block and are polished at an angle. The filter metals are directly coated onto the endface eliminating the need for a lens, thus decreasing the excess loss.

1.1.4 Integrated Optic Couplers

Integrated optic couplers employ waveguides to achieve power transfer rather than optical fibers. These couplers are made in two configurations: multi-layer planar structure and dual side-by-side channel waveguides. Coupling between the two waveguides is caused by optical tunneling. The waveguide technique results in optical interfaces within the coupler that could produce reflections. These interfaces result in long term reliability problems, due to the misalignment between the substrate and optical fiber.

1.2 Fused Biconical Tapered Couplers

There are several methods for manufacturing couplers as listed in section the 1.1. However with an increase in the demand for passive fiber optic couplers fused biconical tapered technique has emerged as the most reliable technique. The widespread use of the fused biconical tapered technique can be attributed to the fact that it is a convenient method of manufacturing couplers and suitable for mass production of environmentally stable couplers. Moreover fused biconical tapered technique can be adapted to a wide range of applications and specifications relatively easily. FBT couplers of up to 100 ports have been manufactured in the past [4].

The couplers are manufactured by twisting a bundle of fibers depending on the port count as shown in the Figure 2b. The twisted bundle is then heated to very high temperatures and tapered by applying axial tension on the bundle. The tapering of the bundle reduces the radius of the individual fibers and the core itself, thus reducing the normalized frequency number of the fiber. The normalized frequency of the fiber is given by

$$V = \frac{2\pi a}{\lambda} NA, \quad (1.5)$$

where NA is the numerical aperture, 'a' is the radius of the core, and 'λ' is the wavelength of operation. The number of bound modes traveling in the core of a step-index fiber is given by

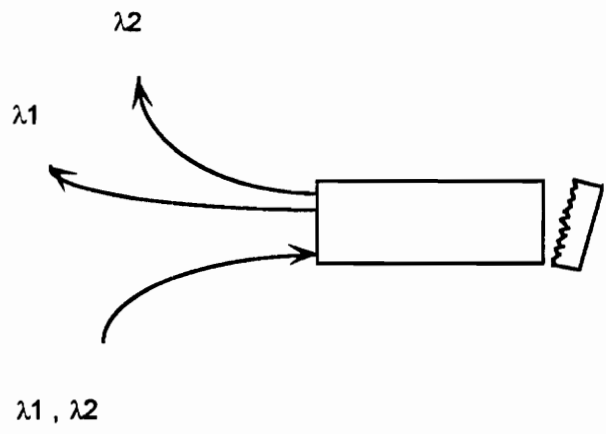


Figure 2a. Diffraction grating coupler with grating on a graded index lens.

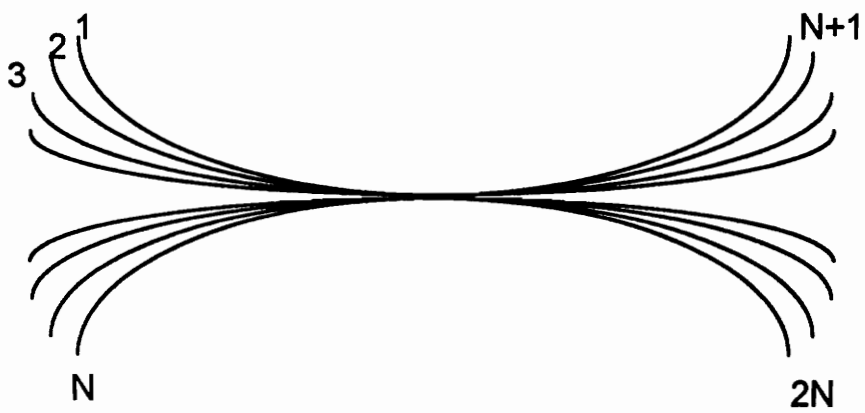


Figure 2b. A fused biconical tapered coupler.

$$M = \frac{V^2}{2}. \quad (1.6)$$

Since the number of bound modes traveling in the core is directly proportional to the normalized frequency number (V-number) of the fiber, the total number of bound modes in the core decreases with a decrease in core radius. The higher-order modes are no longer supported in the core, thus enabling power transfer into the other fibers. The tapering thus serves two purposes, that of reducing the distance between the cores, allowing for greater coupling and reducing the power guided in the throughput core.

1.3 Coupler Parameters

The parameters describing the optical couplers are described below. The transmission efficiency is the ratio of the total amount of output power in all ports to the total amount of input power.

$$\eta = \frac{\sum_j O_j}{\sum_j I_j}, \quad (1.1)$$

where η is the efficiency of coupling

$\sum_j O_j$ is the sum of the power in the output ports', and

$\sum_j I_j$ is the input power in the throughput port before coupling.

The fraction of power lost can be expressed in terms of efficiency of coupling

$$\Lambda = 1 - \eta, \quad (1.2)$$

which is used to find out the excess loss of the device.

$$L = -10 \log \eta, \quad (1.3)$$

where Λ is the fraction of power lost and L is the excess loss. The uniformity of the coupler is given by

$$\text{Uniformity} = \text{IL}_{\max} - \text{IL}_{\min}, \quad (1.4)$$

where IL is the insertion loss of the coupler given by $10\log(P_{\text{out}}/P_{\text{in}})$.

1.4 Uniformity improvement techniques

The fusing and tapering of fibers in the fused biconical tapered technique however does not remove all of the guided power from the input core. The throughput fiber has about 50% more power propagating in the core after the coupler is manufactured when compared to the other cores because the lower-order modes are still confined to the core. For a one hundred port star coupler low excess loss was achieved but uniformity variation was 8 dB [4]. This non-uniformity among ports is a problem that has to be overcome in order to efficiently distribute optical power.

The one obvious problem of the fused biconical tapered couplers is that the port-to-port variations are very large because of their modal dependency. For star couplers, distributed optical power uniformity is important to enable using narrow dynamic range receivers,

which are usually cheaper than wide range receivers. Various methods have been demonstrated in the past in order to decrease the modal dependency of the couplers. Murphy [13,14] demonstrated the improvement in the uniformity of the multimode couplers by modifying the minimum taper region. Three modifications described below are aimed at decreasing the bound power in the throughput core.

1) Push-pull method.

In this method the fibers are fused and tapered to form the minimum taper region. The minimum taper is then pushed together to form a ball in the taper as shown in Figure 3, and then pulled apart. The push-pull technique helps in improving the uniformity of the coupler by reducing the bound power in the throughput core.

2) Score and break method.

The coupler is cleaved at the minimum taper region. The two halves of the coupler are then aligned and fused together. This method misaligns the core of the throughput fiber, so that the throughput core is no longer the core with the maximum power.

3) S-Bend method.

This modification involves the forming of a s-bend in the minimum taper region by pushing the coupler tapering stage together after the minimum taper region is formed as shown in Figure 4. This s-bend causes losses in the throughput core which is then coupled into the other fiber cores.

Another form of improving uniformity of multimode multiport couplers is by the mixer rod method [10]. The fibers are fused and cleaved in the middle of the minimum taper region and a grin lens is placed in between the two sections of the coupler as shown in Figure 5. The light traveling in the injected port travels as cladding and core modes in the contracting taper and as the radius of the core decreases along the taper, modes confined in the core are converted to cladding modes. The converted modes are mixed in the contracting taper and the mixer rod and reconverted in the expanding taper. The light in the mixer rod is redistributed evenly into all ports. The non-converted modes are mixed in the mixer rod and coupled into the expanding taper as both core and cladding modes in all ports of the coupler. The cladding modes are coupled into the other fibers as they propagate in the expanding taper.

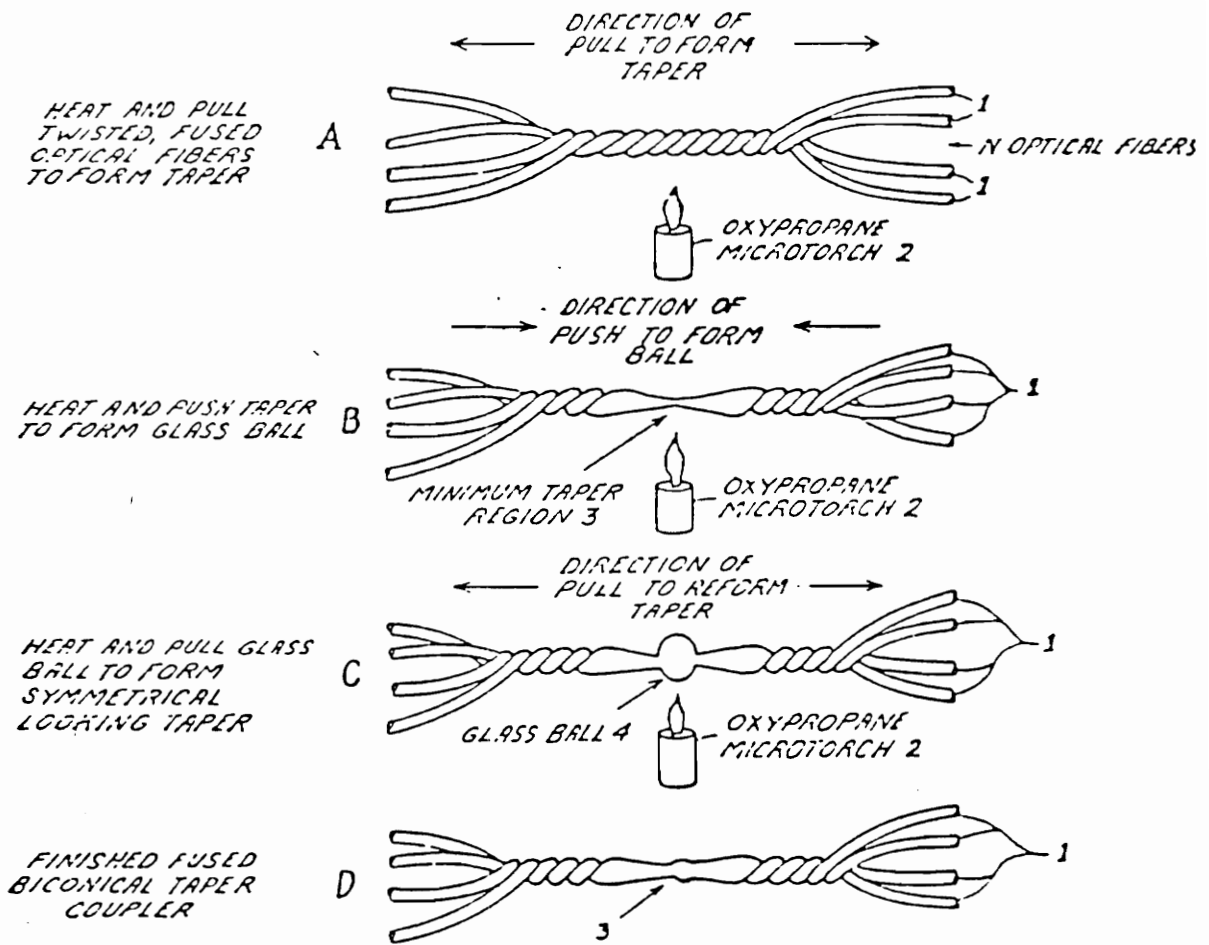


Figure 3. Push-pull method for improvement of uniformity (from Murphy [14]).

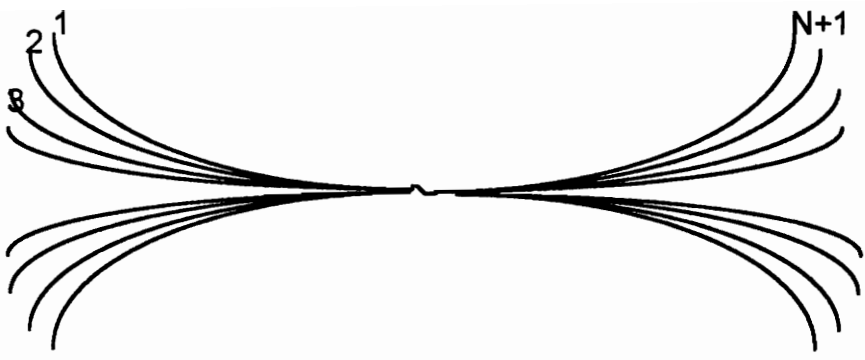


Figure 4. The s-Bend method for improvement of uniformity of couplers (from Murphy [14]).

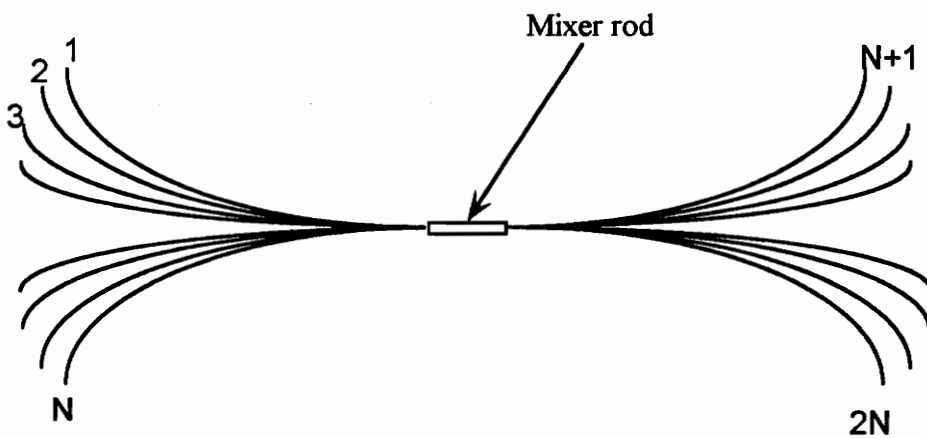


Figure 5. The mixer rod method for uniformity improvement (from Ohshima [10]).

2.0 Theory

The analysis of graded-index multimode fibers using the ray approach, power coupled into the core and cladding of the fiber, and distribution of the power in the core and cladding as the fiber is tapered are discussed in this chapter. The ray equations of motion for general graded-index fibers are described. The ray equations are solved to obtain ray paths and the eigenvalue equation for parabolic profile.

A typical optical fiber has a high refractive index (RI) core surrounded by a cladding of lower refractive index. There are various refractive index profiles (RIP) such as are step-index, graded-index profile, W-clad profile, and others as shown in Figure 6. The step-index fiber has a profile in which the RI of the core is uniform, and the cladding RI is

lower than the RI of the core. The graded-index fiber has a RI in the core that decreases from a maximum in the core to a constant at the core-cladding interface. The power law relationship is used to construct the refractive index variation in the core. The variation of

$$n(r) = \begin{cases} n_1 \left[1 - 2\Delta \left(\frac{r}{a} \right)^\alpha \right]^{1/2} \\ n_1 (1 - \Delta)^{1/2} \end{cases}, \quad (2.1)$$

the refractive index in the multimode fiber with the radius for different power law profiles is shown in Figure 7 [15].

The profile of the core has an effect on the distribution of the power guided in the core and on the overall loss encountered in the fiber. The propagation constants of the various modes traveling in the fiber are dependent on the profile of the core. The parabolic profile of the fiber nearly equalizes the group velocities of the propagating modes. In analyzing multimode fibers we make the following assumptions:

- i) The index profile is circular symmetric.
- ii) The core diameter measures hundredths of wavelengths and so a great number of modes can propagate.
- iii) Index variations within the distance of a wavelength are negligible and the geometric optics apply.
- iv) An ideal case of uniform loss, absence of coupling, and simultaneous excitation of all propagating modes at the input.

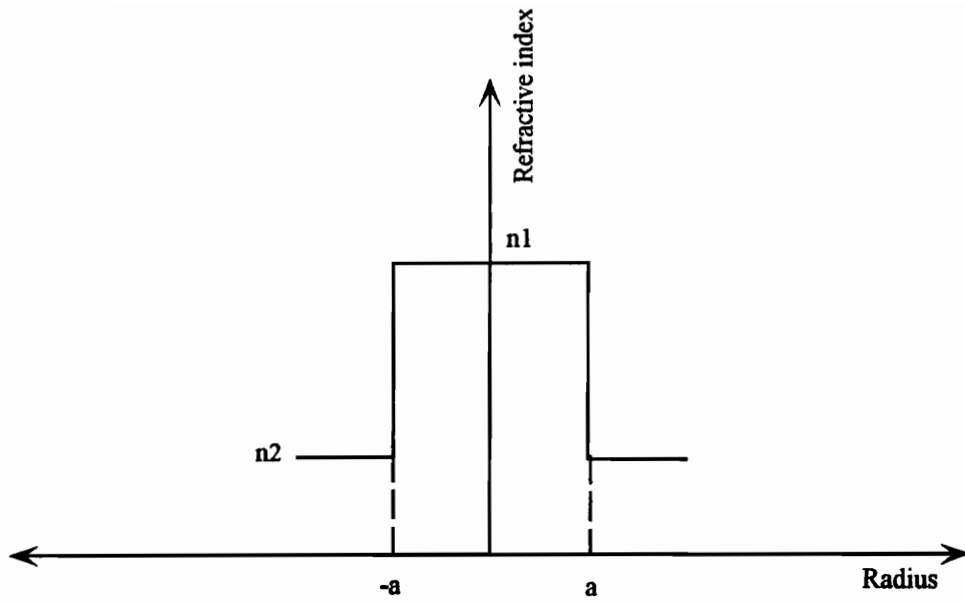


Figure 6a. Refractive index profile of step-index fiber.

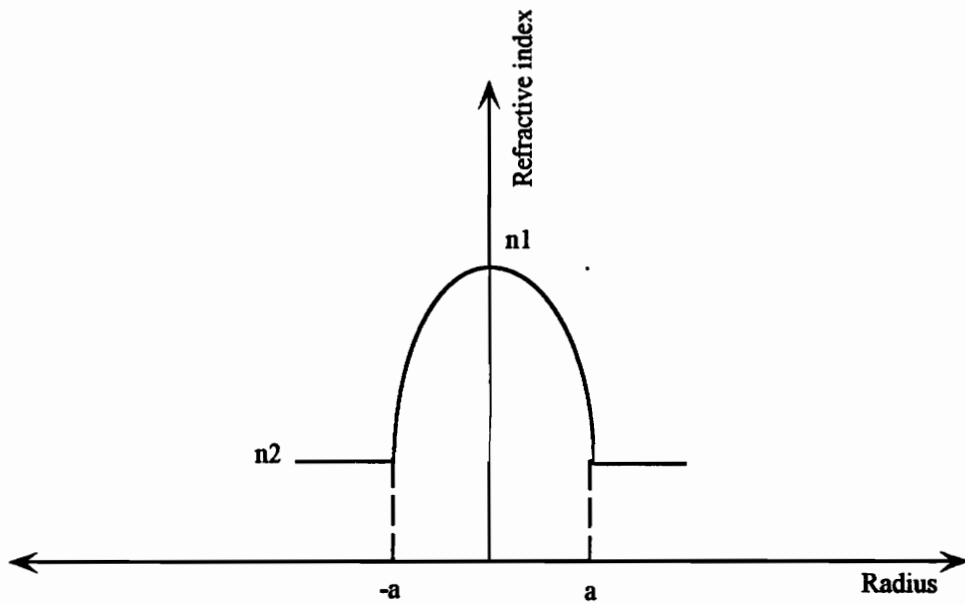


Figure 6b. Refractive index profile of graded-index fiber.

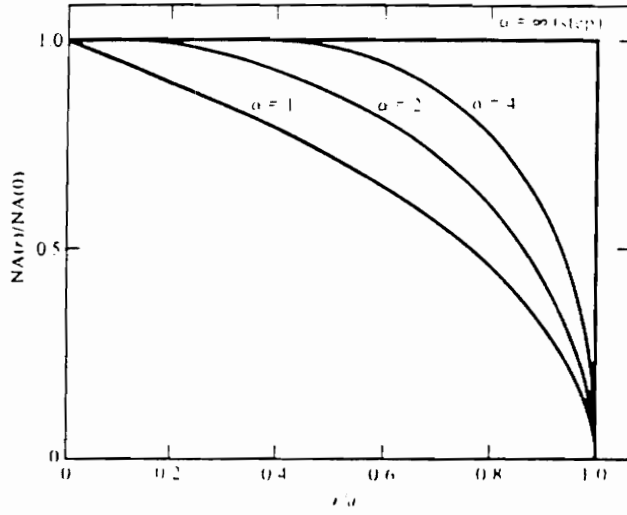


Figure 7. Variation of refractive index profile of the fiber for various ' α ' profiles (from G. Keiser [15]).

2.1 Ray Analysis of Multimode Fibers

Consider the scalar wave equation

$$\Delta^2 \psi + k^2 n^2(r) \psi = 0, \quad (2.2)$$

where

k is wave number,

$n(r)$ is the refractive index, and

ψ is the transverse field component.

For very small wavelengths, i.e. large 'k' solutions for Ψ are of the form

$$\psi(r, \theta, z) = \psi_0(r, \theta, z) e^{-iks(r, \theta, z)}, \quad (2.3)$$

where ψ_0 and s are assumed slowly varying over a wavelength of radiation. Substituting Equation (2.3) into Equation(2.2) we get an expression that has a k^2 term, which becomes the dominant expression for small wavelengths. The resultant expression is:

$$(\nabla s)^2 = n^2(r), \quad (2.4)$$

which is known as the Eikonal equation [16]. This equation determines the propagation in the geometrical optics application since the surfaces $S(\gamma, \theta, z) = \text{const.}$ are the phase fronts. Following Adams [16] let 's' be the distance along the ray path to the point 'r', then the unit vector

$$\hat{u} = \frac{dr}{ds}, \quad (2.5)$$

is tangential to the ray and normal to the phase fronts. We also obtain a vector perpendicular to the phase fronts by taking the gradient of 'S' and from Equation (2.4) we get vector $v = \nabla s$ of length 'n' which is,

$$n \frac{dr}{ds} = \nabla s. \quad (2.6)$$

Differentiating both sides of equation (2.6) with respect to 's' and simplifying yields:

$$\frac{d}{ds} \left(n \frac{dr}{ds} \right) = \frac{1}{2n} \nabla n^2 \quad (2.7)$$

Hence the ray equation that defines the path taken by the ray in the core is:

$$\frac{d}{ds} \left(n \frac{dr}{ds} \right) = \nabla n. \quad (2.8)$$

The eigenvalue equation can be obtained by writing the ray equation in cylindrical polar co-ordinates and simplifying. Writing the above equation in cylindrical polar co-ordinates, and since 'n' is a function of 'r' only the above equation reduces to

$$\frac{d}{ds} \left[n \left(\frac{dr}{ds} \hat{r} + r \frac{d\theta}{ds} \hat{\theta} + \frac{dz}{ds} \hat{z} \right) \right] = \frac{dn}{dr} \hat{r}, \quad (2.9)$$

where \hat{r} , $\hat{\theta}$, \hat{z} are unit vectors in the r, θ , z direction respectively. Equating the 'z' component on both sides of the equation we get:

$$\begin{aligned} \frac{d}{ds} \left[n(r) \frac{dz}{ds} \right] &= 0 \\ n(r) \frac{dz}{ds} &= \text{constant} = \bar{\beta} \text{ (assume)}. \end{aligned} \quad (2.10)$$

Figure 8 shows the ray components in a graded-index fiber that enables us to calculate the ray invariant $\bar{\beta}$ in terms of refractive index [16].

From Figure 8 it can be seen that ' γ ' is the angle between the z axis and the ray direction.

Substituting this relationship into Equation (2.10) we get

$$\bar{\beta} = n(r) \cos\gamma. \quad (2.11)$$

Equation (2.11) can be written as

$$\frac{d}{ds} = \frac{\bar{\beta}}{n} \frac{d}{dz}. \quad (2.12)$$

The Eqn. (2.10) becomes

$$\frac{d}{dz} \left[\frac{dr}{dz} \hat{r} + r \frac{d\theta}{dz} \hat{\theta} \right] = \frac{n}{\bar{\beta}^2} \frac{dn}{dr} \hat{r}. \quad (2.13)$$

The derivatives with respect to 'z' of unit vectors \hat{r} , $\hat{\theta}$, \hat{z} should be known to solve the above equation for $\bar{\beta}$. \hat{r} and $\hat{\theta}$ can be written in terms of i and j, cartesian unit vectors,

$$\begin{aligned} \hat{r} &= \cos\theta i + \sin\theta j \\ \hat{\theta} &= -\sin\theta i + \cos\theta j. \end{aligned} \quad (2.14)$$

Differentiating Eqn.(2.14) with respect to 'z' and substituting the resulting expression into Eqn.(2.12) we get

$$r \ddot{r} + 2 \dot{r} \dot{\theta} \hat{\theta} + r \ddot{\theta} \hat{\theta} - r \dot{\theta}^2 \hat{r} = \frac{n}{\bar{\beta}} \frac{dn}{dr} \hat{r}. \quad (2.15)$$

By separating the r and θ components in Equation (2.15) and integrating the θ component we obtain the second ray invariant:

$$r^2 \dot{\theta} = \text{const.} = \frac{a\bar{l}}{\beta} \quad (\text{assume}). \quad (2.16)$$

From Figure 8 above we have

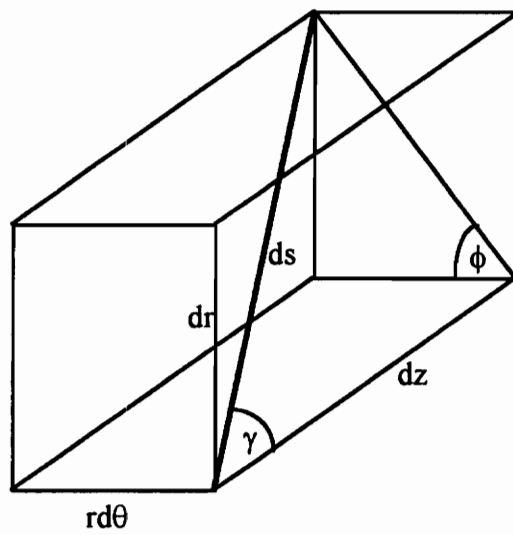


Figure 8. Ray components in a graded-index fiber (from Adams [16]).

$$\begin{aligned} \dot{r} - r\dot{\theta}^2 &= \frac{n}{\beta} \frac{dn}{dr} \\ 2r\dot{\theta} + r\ddot{\theta} &= 0. \end{aligned} \quad (2.17)$$

A differential equation for the ray trajectory can be obtained by substituting Equation (2.17) into Eqn. (2.15)

$$\dot{r} - \left(\bar{l} \frac{a}{\bar{\beta}} \right)^2 \frac{1}{r^3} = \frac{1}{2\bar{\beta}^2} \frac{dn^2}{dr}, \quad (2.18)$$

where \bar{l} and $\bar{\beta}$ are the constants of motion. Integrating Equation (2.18) with respect to 'r' we get

$$\dot{r}^2 + \left(\bar{l} \frac{a}{\bar{\beta}} \right)^2 \frac{1}{r^2} = \frac{n^2}{\bar{\beta}^2} + c, \quad (2.19)$$

where c is a constant of integration. The constant 'c' can be solved for by observing from Figure 8 that

$$\begin{aligned} dr &= ds \sin\gamma \sin\phi \\ &= dz \tan\gamma \sin\phi \end{aligned} \quad (2.20)$$

Solving Equations (2.17), (2.11) and (2.19) we obtain a value for c, which is -1. Equation (2.19) can be written as

$$\frac{dr}{dz} = \frac{1}{\bar{\beta}} \left[n^2(r) - \bar{\beta}^2 - \left(\frac{a\bar{l}}{r} \right)^2 \right]^{1/2}. \quad (2.21)$$

Combining Eqns. (2.21) and (2.16) we get:

$$\frac{d\theta}{dr} = \frac{a\bar{l}}{r^2} \left[n^2(r) - \bar{\beta}^2 - \left(\frac{a\bar{l}}{r} \right)^2 \right]^{1/2}. \quad (2.22)$$

The ray invariants $\bar{\beta}$ and \bar{l} can be written in terms of modal components.

$$\begin{aligned} \bar{\beta} &= \frac{\beta}{k}, \\ \bar{l} &= \frac{l}{ak}, \end{aligned} \quad (2.23)$$

Thus Equation (2.22) can be written in terms of modal components,

$$\frac{d\theta}{dr} = \frac{1}{r^2 k} \left[k^2 n^2(r) - \beta^2 - \left(\frac{l}{r} \right)^2 \right]^{1/2}. \quad (2.24)$$

The Equations (2.22) and (2.24) can be used to calculate the ray paths in graded-index fibers. We define

$$q^2 = k^2 n^2(r) - \beta^2 - \left(\frac{l}{r} \right)^2. \quad (2.25)$$

The function 'q' has zeros at radii r_1 and r_2 , which are known as the caustic radii, and which define the inner and outer caustics. For a bound ray the projection of the ray path on the (r, θ) plane remains in between the caustic surfaces as shown in Figure 9 [16].

The radii of the caustic surfaces can be obtained by solving Eqn.(2.25), and are given by:

$$\left(\frac{r_1}{a} \right)^2 = \frac{u^2 \pm (u^4 - 4v^2 l^2)^{1/2}}{2v^2}. \quad (2.26)$$

The eigenvalue equation can be obtained by geometric optics derivation. Following Gloge and Marcatili [18] the ray traveling in the core experiences a phase change every time it

changes direction. The total transverse phase change in one ray period should be an integral multiple of 2π :

$$2 \int_{r_1}^{r_2} q \, dr - \delta_1 - \delta_2 = 2N\pi \quad (N = 0, 1, 2, \dots), \quad (2.27)$$

where δ_1 and δ_2 are phase shifts suffered by the ray at the caustic surfaces and $\delta_1 = \delta_2 = \pi/2$. The Eigenvalue equation thus becomes [16]:

$$\int_{r_1}^{r_2} \left(k^2 n^2(r) - \beta^2 - \frac{l^2}{r^2} \right)^{1/2} dr = \left(N + \frac{1}{2} \right) \pi \quad (N = 0, 1, 2, \dots). \quad (2.28)$$

By solving the above Eigenvalue integral with the integration limits from Eqn.(2.26) [16] we obtain:

$$u^2 = 2v(2N + l + 1), \quad (2.29)$$

where $N = 0, 1, 2, \dots$ and $l = 0, 1, 2, \dots$. The total number of modes propagating in the core of the graded-index fiber can be estimated from the above equation. The Figure 10 given below is a plot of l/v and N/v from Eqn.(2.29) [16]. The total number of guided modes is given by the area enclosed by the cut-off line $u/v = 1$. Figure 11 shows the propagation constant of the modes as a function of normalized frequency [19].

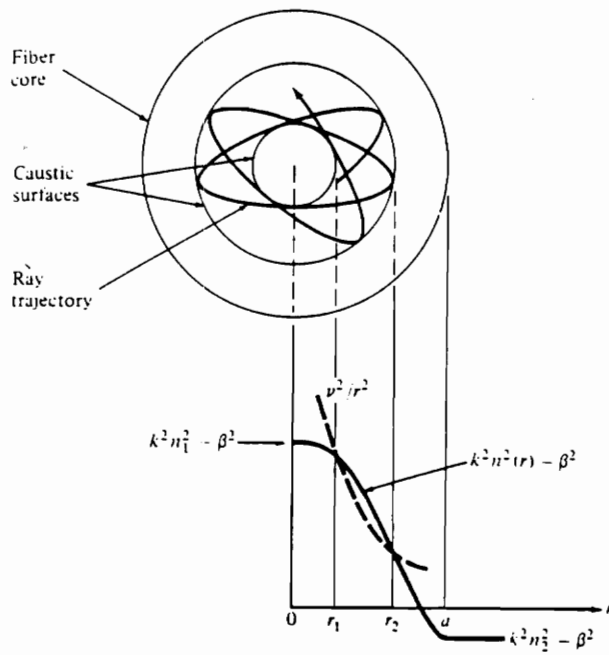


Figure 9. Cross sectional projection of a ray in a graded-index fiber (from G. Keiser [15]).

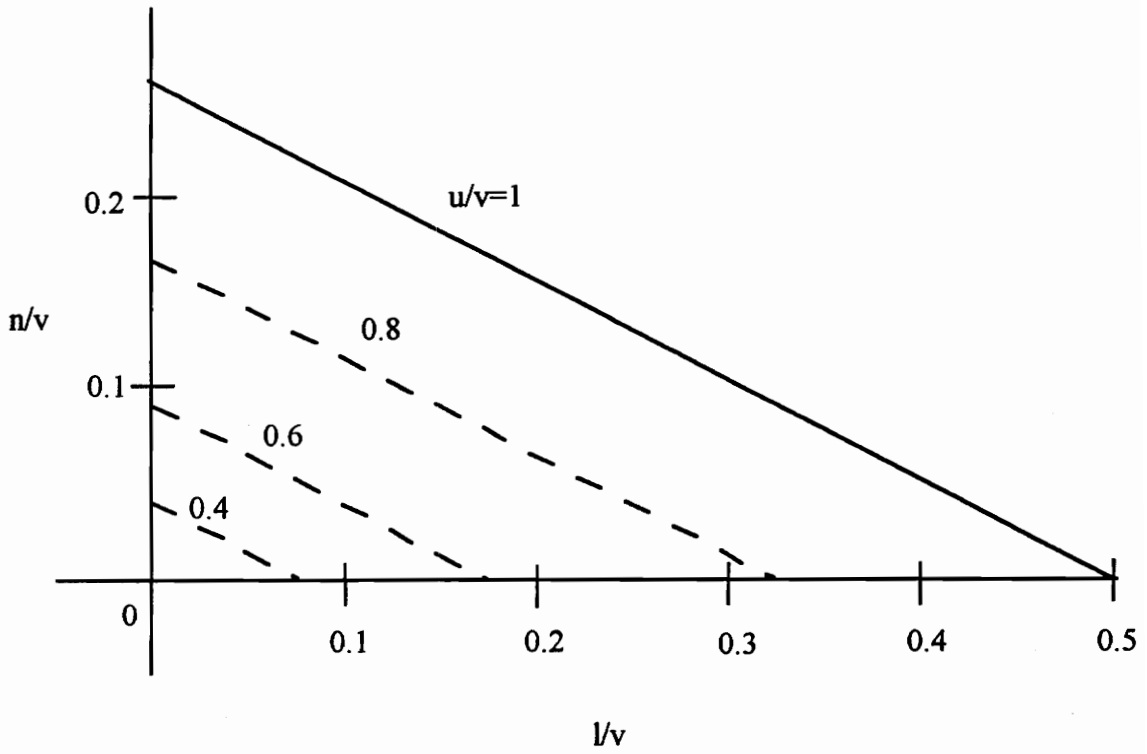


Figure 10. Plot of l/v and N/v (from M.J. Adams [16]).

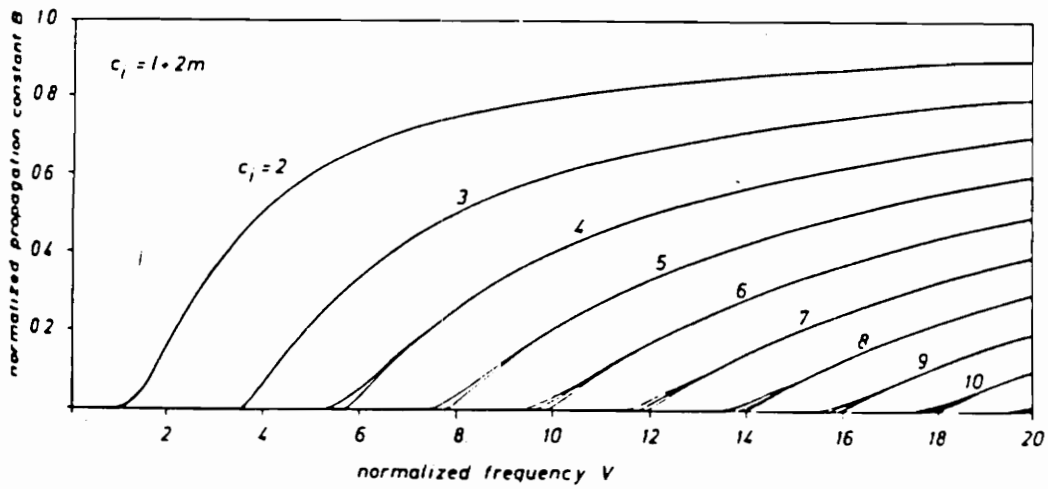


Figure 11. Propagation constant of the modes as a function normalized frequency (from Gloge et al. [19]).

2.2 Variations in Bound Power with Normalized Frequency

The relation between the portion of power bound in the core, normalized propagation constant, and normalized group delay can be obtained from Brown's Identity [17]:

$$\frac{1}{v_g v_p} = \frac{d\beta^2}{d\omega^2} = \frac{1}{c^2} \frac{\int n^2 S_z dx dy}{\int S_z dx dy}, \quad (2.30)$$

where v_g and v_p denote group and phase velocity respectively, n is refractive index, and S_z is the axial component of the time averaged Poynting vector. Normalized propagation constant is given by:

$$B = \frac{(\beta / k)^2 - n_2^2}{n_1^2 - n_2^2}. \quad (2.31)$$

Following Krumbholz et. al. [17] the left hand side of Brown's Equation can be written as

$$c^2 \frac{d\beta^2}{d\omega^2} = c^2 \frac{d\beta}{d\omega} \frac{\beta}{\omega} = \frac{1}{2} (n_1^2 - n_2^2) \left(\frac{d(VB)}{dV} + B \right) + n_2^2. \quad (2.32)$$

The right hand side of Brown's Identity can be written as:

$$\frac{\int n^2 S_z dx dy}{\int S_z dx dy} = n_1^2 \rho_{core} + n_2^2 \rho_{clad} - 2\Delta n_1^2 \frac{\iint_{core} S_z R dR d\phi}{\iint S_z R dR d\phi}, \quad (2.33)$$

where $R = r/a$ is the normalized radial coordinate and

$$\rho_{core} = \frac{\int_{core} S_z dx dy}{\int S_z dx dy} = \frac{P_{core}}{P_t}, \quad (2.34)$$

$$\rho_{clad} = \frac{\int_{clad} S_z dx dy}{\int S_z dx dy} = \frac{P_{clad}}{P_t}.$$

Using Equations (2.34) and (2.32) we obtain:

$$\rho_{core} = \frac{1}{2} \left(\frac{d(VB)}{dV} + B \right) + \frac{a^2 \int \int_{core} S_z R^{\alpha+1} dR d\phi}{P_{core} + P_{clad}}. \quad (2.35)$$

The fraction of power in the core can be calculated by eliminating the integral in the above equation and can be achieved by considering the scalar wave equation:

$$\frac{1}{R} \frac{d}{dR} \left(R \frac{dF}{dR} \right) + \left(u^2 - v^2 R^\alpha + \frac{l^2}{R^2} \right) F = 0, \quad (2.36)$$

where $F(R)$ is the radial dependence of the electric field which is of the form:

$$E = E_0 \cos(l\phi) \frac{F(R)}{F(1)} \exp(-j\beta z). \quad (2.37)$$

Multiplying equation (2.36) with $R^2(dF/dR)$ and integrating within the limits $0 < R < 1$, and eliminating terms by making use of the characteristic equation:

$$\left[\frac{1}{F} \frac{dF}{dR} \right]_{R=1} = -W \frac{k_{l-1}(W)}{k_l(W)} - 1 \quad (2.38)$$

we arrive at:

$$\rho_{core} = \frac{\alpha + 2}{2\alpha} \frac{d(VB)}{dV} - \frac{\alpha - 2}{2\alpha} B. \quad (2.39)$$

For a parabolic profile fiber $\alpha=2$, therefore Eqn.(2.39) becomes:

$$P_{core} = \frac{d(VB)}{dV} \quad (2.40)$$

Normalized propagation constant B is defined as

$$B = 1 - \frac{u^2}{v^2} \quad (2.41)$$

Differentiating the above equation with respect to v we get [19]:

$$\frac{d(BV)}{dV} = v^2 - \frac{u^2}{v^2} + \frac{2u}{v} \frac{du}{dv} \quad (2.42)$$

Differentiating Eqn.(2.29) with respect to v we obtain the following Eqn.:

$$\frac{du}{dv} = \frac{(1 + 2m + 1)}{u} \quad (2.43)$$

Combining the Equations.(2.43) and (2.44) we obtain a relation between the fraction of the power bound in the core and the normalized frequency number. Figure 12 shows the power flow in the core versus the normalized frequency. When light is launched into a fiber it travels both in the core and the cladding. As can be seen from Figure 11 the number of modes propagating in the core decreases with a decrease in the normalized frequency number of the fiber. As the coupler is tapered the radius and V-number of the fiber decreases thus reducing the number of modes confined to the core. This in turn reduces the amount of bound power traveling in the core of the fiber as can be seen from Figure 12. The modes that are no longer supported in the core because of the reduced radius, are converted to cladding modes and propagate in the cladding. The converted modes are coupled back into the remaining cores in the up-taper region thus causing coupling.

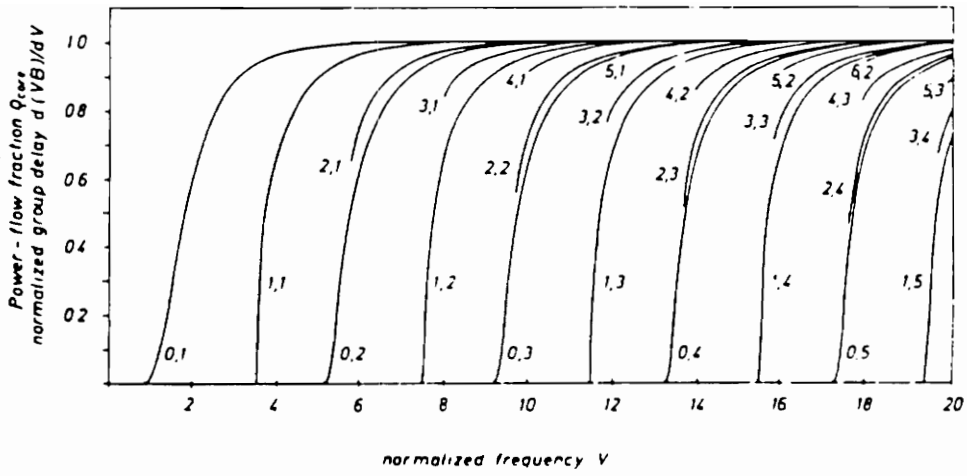


Figure 12. Power flow in the core versus the normalized frequency number (from Krumbholz et al [17] for $\alpha=2$).

3.0 Diffusion

Optical fibers are typically made of either glass, plastic or sapphire. Plastic optical fibers are used in short distance applications which do not need low-loss fibers and in harsh environments where the strength of plastic fibers have an advantage over the use of glass fibers. Glass fibers due to their low attenuation are used for long-haul applications.

Glass which is made by fusing mixtures of metal oxides, sulfides or selenides is a randomly connected molecular network rather than a well defined ordered structure as in crystalline materials. Because of its molecular structure glass does not have a definite melting point. Glass retains its structure upto a several hundred degrees centigrade and if the temperature

is increased further it forms a viscous liquid. The melting point of glass is an extended range of temperatures. Glass composed of pure silica is referred to as either silica glass, fused silica, or vitreous silica. Optical fibers are made of glass consisting of either silica or silicate. The principal raw material for silica is sand.

Glass optical fibers are made with oxide glasses, the most common of which is silicon oxide (SiO_2) which has a refractive index of 1.458 at a wavelength of 850 nm. Optical fibers have two distinctive areas, the core and the cladding which have different refractive index but are generally made up of the same basic material to give the fiber its guiding properties. The silica has to be doped with certain impurities in order to raise or lower its refractive index to get the two distinct core, cladding regions. Dopants such as fluorine or other oxides such as germanium, phosphorus, raise or lower the refractive index when added to pure silica. As shown below in Figure 13 the refractive index of the core increases when germanium or phosphorus is added and decreases when fluorine or barium oxide is added [15]. The optical fibers are produced with different compositions and combinations of dopants. The primary dopants are:

- 1) GeO_2 - SiO_2 core ; SiO_2 cladding,
- 2) P_2O_5 - SiO_2 core ; SiO_2 cladding,
- 3) SiO_2 core ; B_2O_3 - SiO_2 cladding,
- 4) GeO_2 - B_2O_3 - SiO_2 core ; B_2O_3 - SiO_2 cladding, and

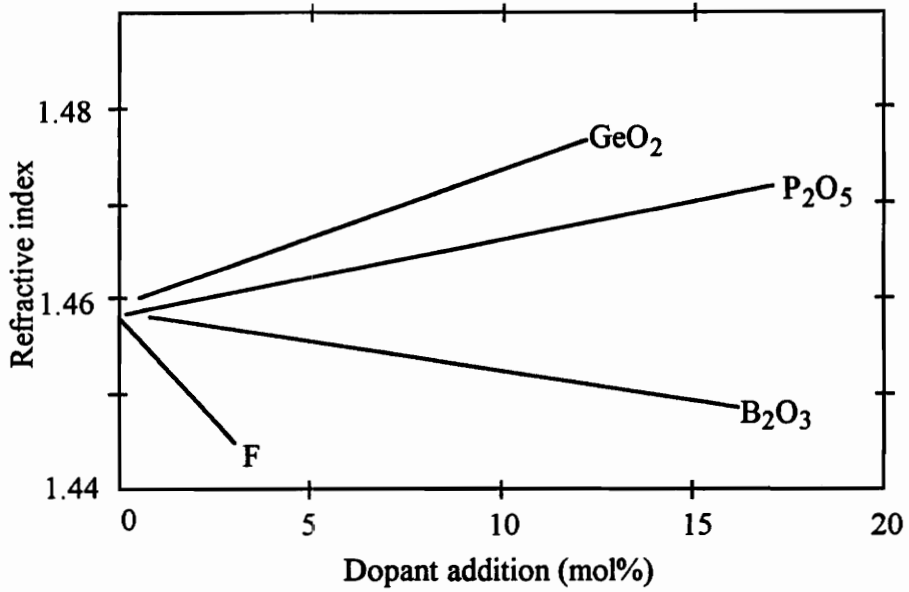


Figure. 13 Variation in refractive index as a function of doping concentration in silica glass (from Keiser [15]).

5) GeO₂-SiO₂ core ; F-SiO₂ cladding.

The phenomenon of migration of dopants when the fiber is heated to very high temperatures is known as diffusion. This phenomenon is attributed to the differential mass transport of the core glass and the undoped cladding glass or the doped cladding glass depending on the optical fiber used. Diffusion of dopants is increased by the axial stress that is applied to the fibers during fusing and tapering. When fibers with dopants in the core are diffused, the dopants from the core spread out into the cladding thus lowering the effective refractive index of the cladding. The migration of dopants results in an increase in the diameter of the core. When fibers with dopants in the cladding are diffused the dopants diffuse into the core thus reducing the effective diameter of the core. Diffusion of dopants either increases (or decreases) the core diameter, and refractive index difference depending (on whether the dopants are in the cladding or the core) on the concentration and composition of the dopants in the fiber. The concentration of the dopants in the fiber during diffusion depends upon the γ which is the product of diffusion constant K , the time of heating t and is given by the equation [20,21],

$$c = a_0 + \sum_{\alpha} a_{\alpha} J_0(\alpha r) \exp(-\alpha^2 \gamma) \quad (r < b), \quad (3.1)$$

where a_{α} is the expansion coefficient, J_0 is the Bessel function of 0 order, r is the radius and b is the cladding radius. The diffusion constant K itself varies with temperature as

$$K = K_0 \exp\left(-\frac{g}{T}\right), \quad (3.2)$$

where K_0 and g are obtained by fitting to experimental data. γ can then be calculated from K . Extensive work in dopant diffusion of single mode fibers and couplers has been done in the past.

Krause et al. [22] studied diffusion in fibers of different concentrations. A sample of $\text{GeO}_2\text{-SiO}_2$ core with a Δ^+ of 0.25% and depressed index deposited cladding of $\text{F-P}_2\text{O}_5\text{-SiO}_2$ with a Δ^- of 0.12% was used for studying the phenomenon. When the fiber is heated to high temperatures the germanium diffuses out of the core and the fluorine diffuses into the core, each phenomenon serving to decrease the refractive index of the core. The effect of diffusion on the refractive index profile of silica core and depressed clad fiber is shown in Figure (7) of [22]. shown below in Figure 14. It can be seen in the figure that as the temperature increases Fluorine diffuses into the core and germanium diffuses out of the core thus decreasing the effective refractive index of the core. This phenomenon was identified as a contributing factor for splice loss.

McLandrich [23] established that the core size and RIP of the fiber is altered during the process of manufacturing couplers. A GeO_2 doped SiO_2 fiber was used to conduct experiments. The Table 1 and Figure (2) from [23] are shown below. As the time of heating the fiber and tapering increase the concentration of GeO_2 in the core decreases. Figure 15 shows the measured GeO_2 concentration as the function of the radial distance

from the center of the fiber. This phenomenon effectively decreases the relative index difference in the fiber while increasing the core radius at the same time.

C.W.Pickett et al. [24] related the losses in a coupler to dopant diffusion. In stress induced high birefringence fibers dopant diffusion occurs with tapering at high temperatures and simultaneous axial tension. The experiments were conducted on fibers with varying conditions of initial birefringence. The Figure 1 for refractive index change from [24] is given below in Figure 16. Fiber P has a higher concentration B_2O_3 of 12.3 and fiber O has a concentration of 9.4. In [24] the core diameter was observed to increase as the taper was formed because of the Ge dopants diffusing out and increasing the refractive index of the surrounding area. Thus if dopant transports are considered separately, B_2O_5 increases the core radius and P_2O_5 decreases the core radius. But when both are present in the core the increase or decrease in the core radius depends on the concentration of dopants.

The technique of expansion of the core using thermal diffusion of dopants is finding widespread use in fields of optical communications and optical sensing. Localized expansion of the core is being used for efficient coupling between singlemode fibers, between fibers and laser diodes, and in optical isolators and filters [30]-[32].

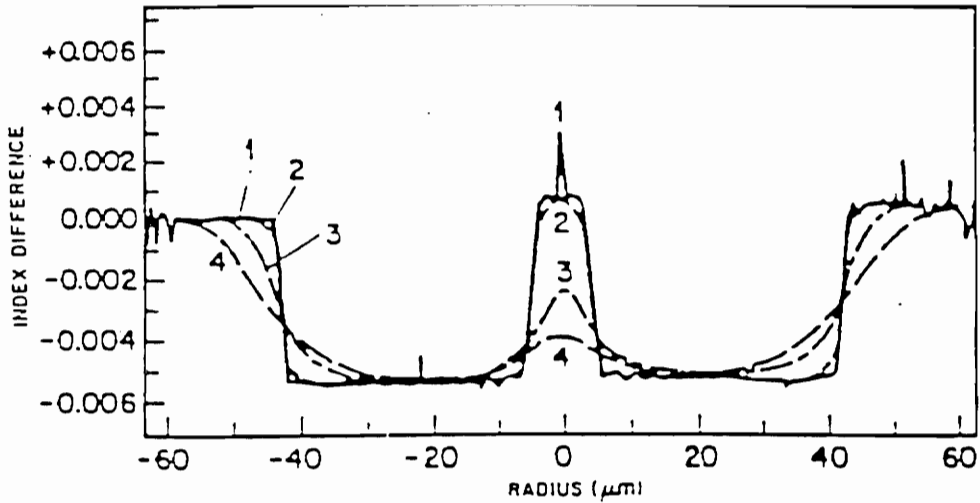


Figure 14. Refractive index profile of silica core fiber. Unheated (1), heated at $\sim 1950^{\circ}\text{C}$ for 6s (2), for 25s (3), and for 40s (4) (from Krause et al. [22]).

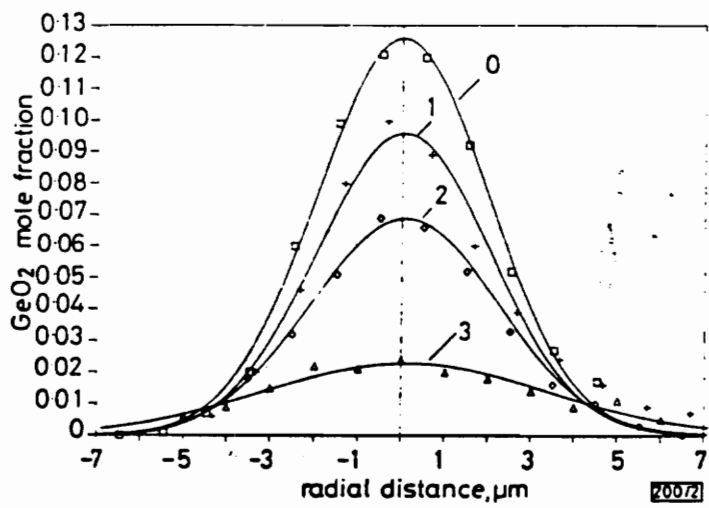


Figure 15. Measured GeO_2 concentration as the function of radial distance from the center of the fiber (from McLandrich [23]).

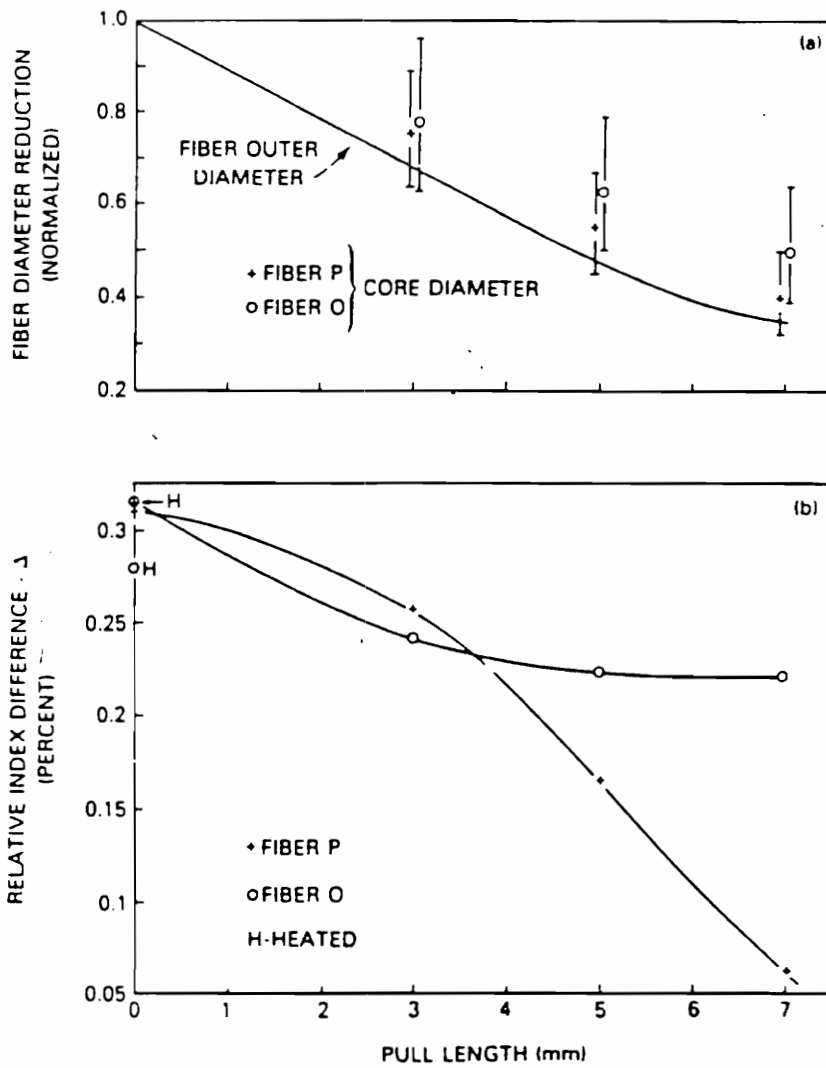


Figure 16. Refractive index change as a function of taper length (from Pickett et al. [24]).

4.0 Coupler Station

Optical couplers are made by fusing two or more fibers together. The output of the ports are monitored and fusing is stopped once the desired splitting ratios are achieved. This process can become laborious if the port count exceeds three. The coupler station that is described in this chapter was developed in order to ease the manufacture of couplers. The coupler station helps in cutting down the cost and time involved in making multiport couplers. Different parts of the coupler station, and the process of the making of the couplers are discussed in this chapter.

The block diagram of the coupler station is shown below in Figure 17. The coupler station has three primary components, the source/detector arrays, the CPU, and the coupler tapering stage.

4.1 Source/Detector Array.

The source/detector array serves a dual purpose of injecting the light into the multimode fiber and detecting the light when the other end of the fiber is injected. The source/detector array is broken down into five different entities, and will be described in detail in the following sections:

4.1.1 The light emitting diode(LED) lens alignment,

4.1.2 Beam splitter,

4.1.3 Fiber lens alignment,

4.1.4 Reference detector, and

4.1.5 Throughput detector.

4.1.1 The Light Emitting Diode (LED) Lens Alignment

A light emitting diode (LED) at 860nm was used as a source in the system because LEDs are inexpensive, compact, easily portable, highly reliable, and require no maintenance. The LEDs are mounted with a spherical lens that focuses the light beam which is of importance to the system.

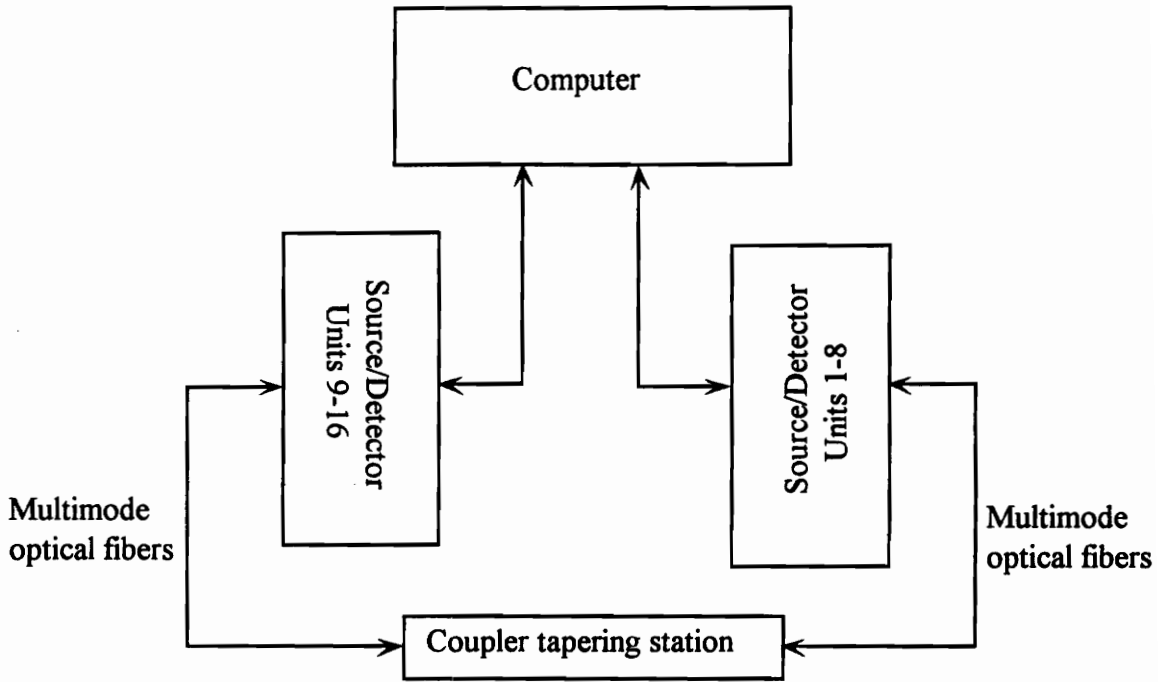


Figure 17. Block diagram of coupler station.

The LED emits a slightly collimated beam which has to be collimated further in order to obtain optimum injection into the fiber. The collimation is achieved with the help of a graded index (GRIN) lens. The GRIN lens is placed at a particular distance from the LED, which is measured in terms of focal length. The GRIN lens has to be placed at a working distance from the LED in order to achieve the necessary collimation. GRIN lenses are identified by their pitches and lens of various pitches are manufactured for different applications. A 0.11 pitch GRIN lens with a 3mm diameter was chosen because it collimates a point source into a 3 mm beam. The distance between the lens and the LED surface can be calculated by the following equation:

$$\text{Working Distance (L)} = \frac{1}{N_0 \times A^{1/2} \times \tan(A^{1/2} \times z)} \quad (4.1)$$

where the parameters

N_0 = index of refraction,

$A^{1/2}$ = Quadratic gradient constant (mm^{-1}),

Z = Length of lens (mm),

P = Pitch of lens,

$$N_0(\lambda) = 1.5477 + (6.37 \times 10^{-3} / \lambda^2),$$

$$N_0(830) = 1.5986,$$

$$A^{1/2} = .2339 + (7.643 \times 10^{-3} / \lambda^2) + (9.757 \times 10^{-4} / \lambda^4) = 0.202 \text{ mm}^{-1},$$

$$Z = 2\pi P / A^{1/2} = 3.42 \text{ mm, and}$$

$$L = 3.7457 \text{ mm.}$$

Therefore the lens has to be placed at a distance of approximately 3.5 mm from the source to achieve good collimation. The lens and LED are inserted in a brass barrel and the distance between the two was set at approximately 3.5 mm as shown in Figure 18. The LED was held in place with the help of 24 hr. curing Bi-Pax Tra Bond epoxy. The lens is fixed to the barrel by Ultra Violet curable adhesive that is optically clear.

4.1.2 Fiber Lens Alignment

This fiber lens alignment makes use of a graded index lens, a large core (200 micron) optical fiber and a brass barrel. The function of the large core diameter is to act as the injecting fiber for the ports of the coupler. The light that is emitted by the LED, and collimated by the GRIN lens has to be coupled into the large core fiber with the minimum loss. This is achieved with a GRIN lens that receives the collimated beam from the source and converts it to a point source on the endface of the fiber. The distance between the lens and the fiber endface has to be calculated for optimum coupling into the fiber. Equation (4.1) is used for calculating the distance between the two. All parameters except the length of the lens remain unchanged. Substituting $Z=7.80$ mm and, $\tan(A^{-1/2} \times Z) = \tan(\pi/2) = \infty$ into Equation (4.1) we get $L = 1/\infty = 0$ mm. Therefore for maximum coupling of light into the fiber the lens should be touching the fiber endface. The fiber is potted in a ferrule with the help of Bi-Pax epoxy and polished. The GRIN lens and the

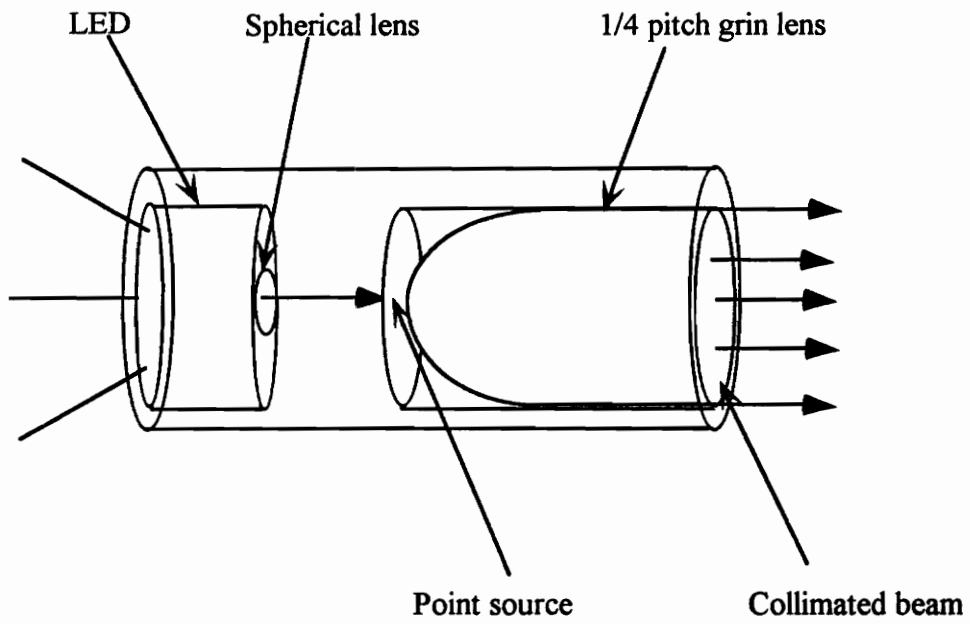


Figure 18. LED/lens assembly in a brass barrel.

ferrule are placed in a brass barrel. The lens is held in place with blue epoxy and the ferrule is fixed to the barrel with the Bi-Pax epoxy. This assembly is shown in Figure 19 below.

4.1.3 Detectors

The source/detector array has two detectors. One of these acts as the reference detector and the other acts as the throughput detector. The Silicon detector was chosen due to the highest quantum efficiency of $\eta = 0.9$ at an operating wavelength 860 nm.

The function of reference detector is to monitor variations in the optical power at the source while the function of the throughput detector is to measure the amount of power being coupled into one port of the coupler. The voltages across the throughput detector, corresponding to the optical power incident on it after the input power into the fiber is split by the coupler, are too low to be read by the A/D card. A trans-impedance amplifier was used to increase the voltage to a 0-5 volt scale which is required by the A/D card. Figure 20 below shows the circuit of the trans-impedance amplifier used. Figure 21 shows the plot of output voltage of the trans-impedance amplifier versus the incident optical power for the throughput detector. Figure 22 shows the plot of output voltage of opamp and incident optical power with LED drive current for reference detector.

The source/detector system is formed by fitting the LED/lens barrel and the fiber/lens barrel into the opposite ends of a Delrin™ box while monitoring the output of the fiber

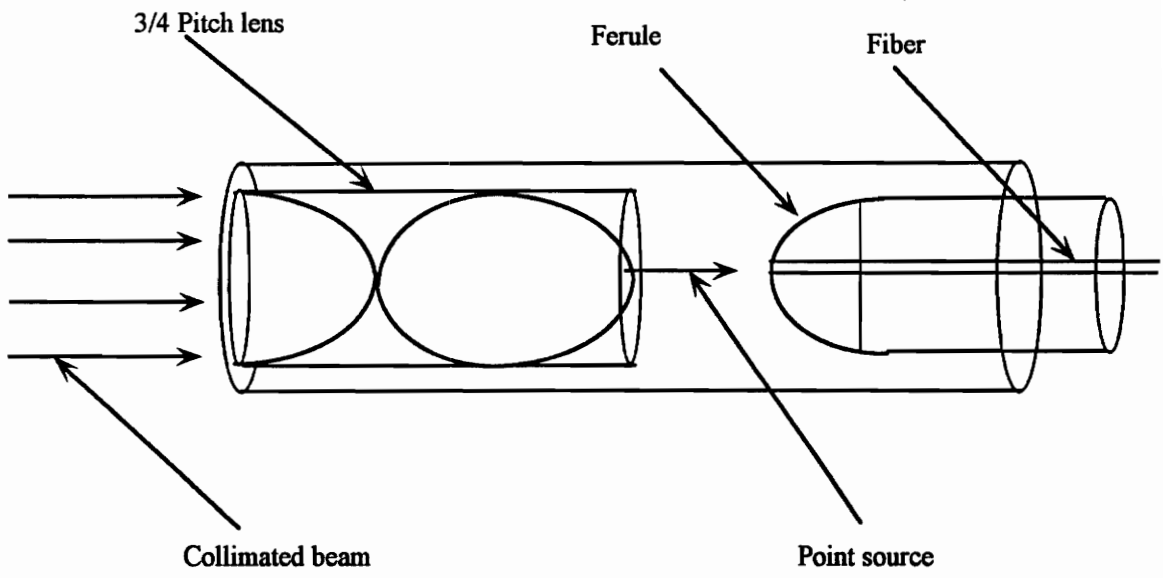


Figure 19. Fiber-lens assembly in a brass barrel.

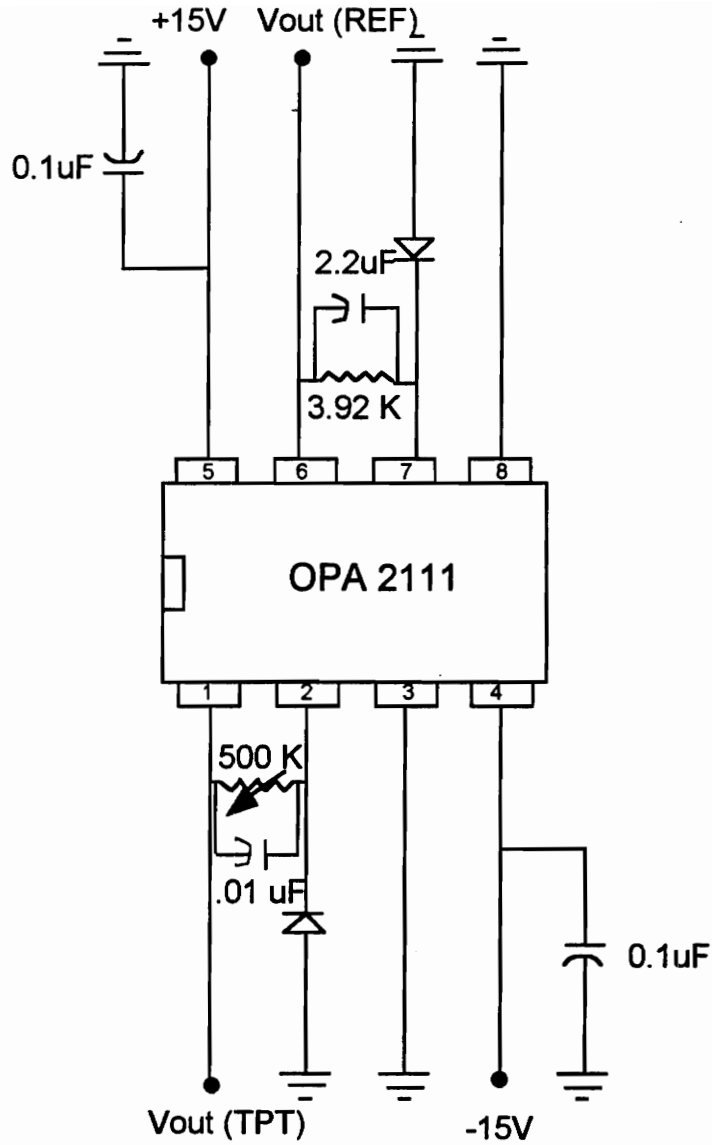


Figure 20. Circuit of the trans-impedance amplifier used for detectors.

as shown in Figure 23 below. A beam splitter is inserted into the box in between the two barrels. The barrels are adjusted in the box till the optimum power is injected into the fiber.

The function of the beam splitter is to split the light beam from the source so that a part of the beam is incident on the reference detector to detect source fluctuations. It also splits the throughput beam from the fiber so that a part of the light beam from the port of the coupler is incident on the throughput detector. The reason for choosing a beam splitter instead of a coupler is that a beam splitter is modally independent while FBT couplers are not. If the coupler inside the system transmits the higher order modes only, then the uniformity of the coupler being manufactured would be modally dependent. The box that houses all these components is made of thermoplastic (Delrin™) and was used because of its insulating property and easy machinability.

The most critical test of the source/detector array is the modal dependency of the system. The power injected into the fiber from the source/detector array has to be equally distributed among all modes. The importance of the modal power distribution is to provide a source for the coupler that is modally independent so that the coupler manufactured is modally independent. The assembled source/detector system was tested for modal dependency by the experimental setup shown in Figure 24. Since the diameter of the injecting fiber was larger than the coupler multimode fiber, more modes in the

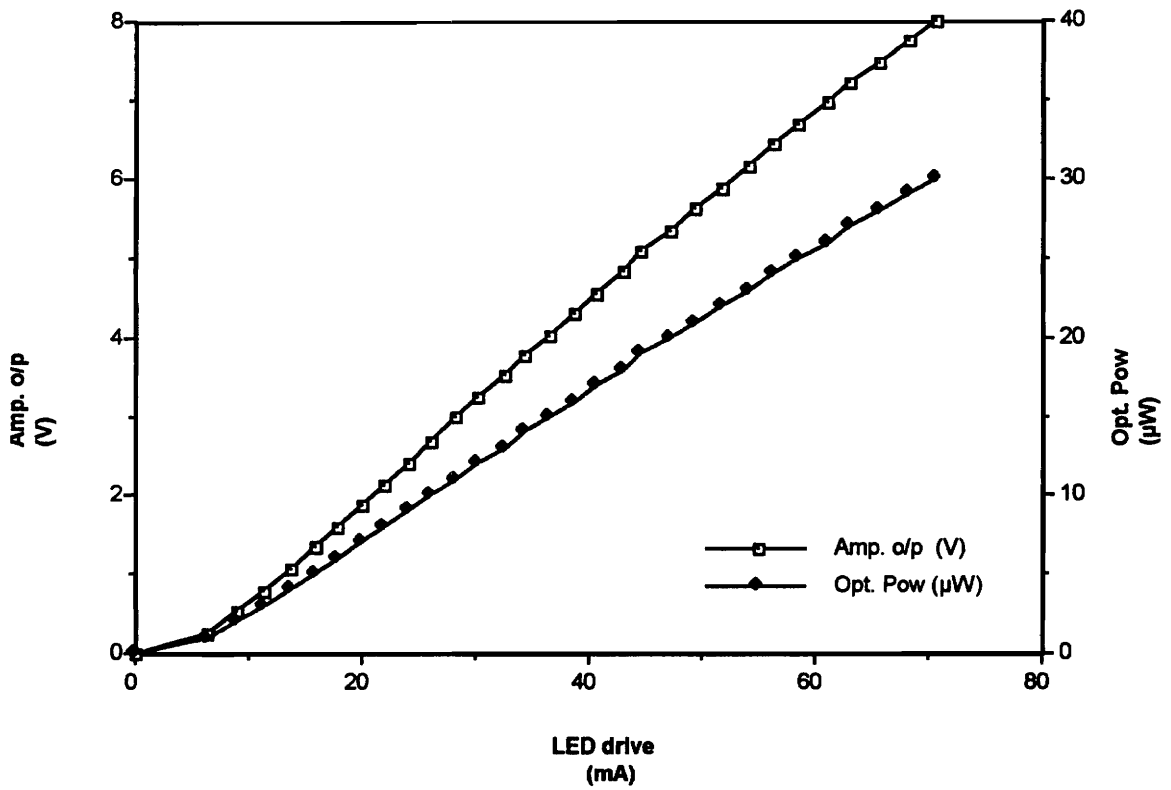


Figure 21. Plot of output voltage of the trans-impedance amplifier versus the incident optical power for the throughput detector.

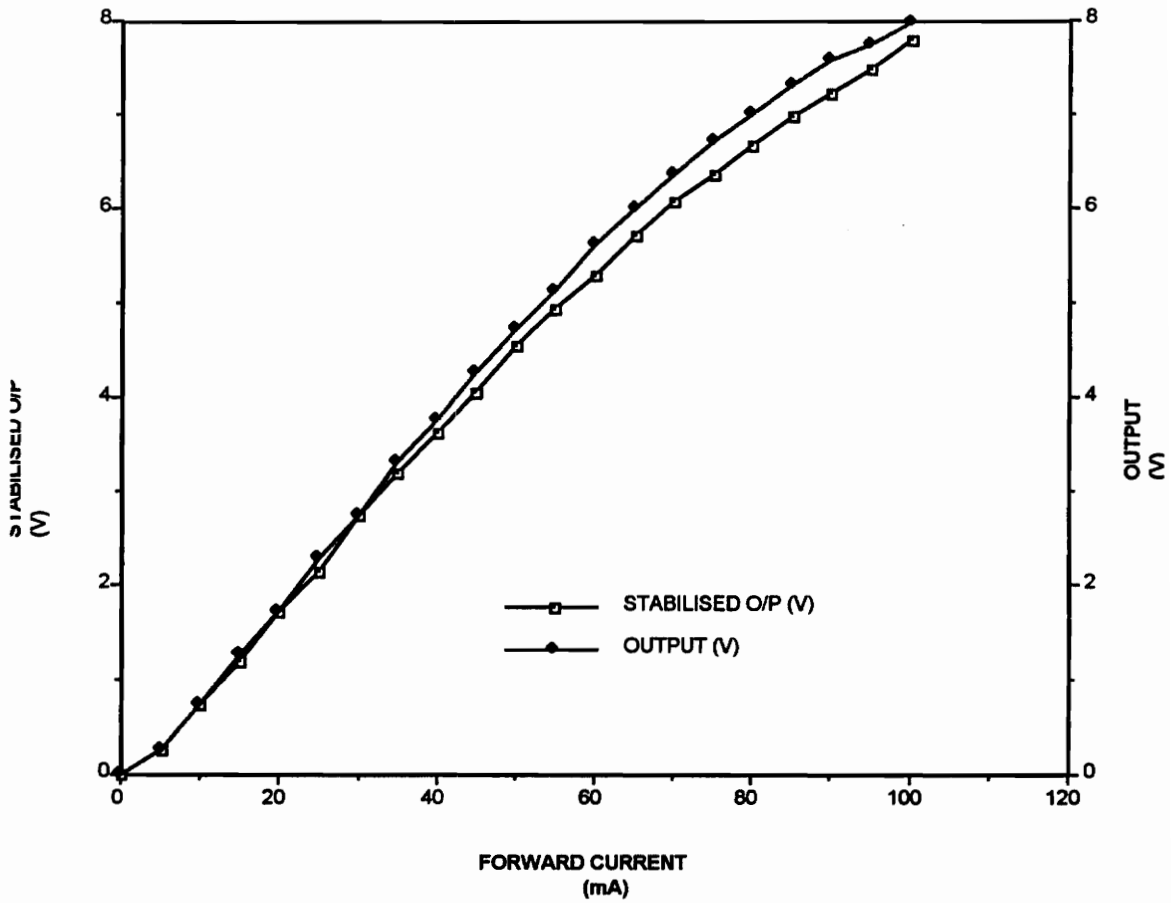


Figure 22. Plot of output voltage of opamp and incident optical power with LED drive current for reference detector.

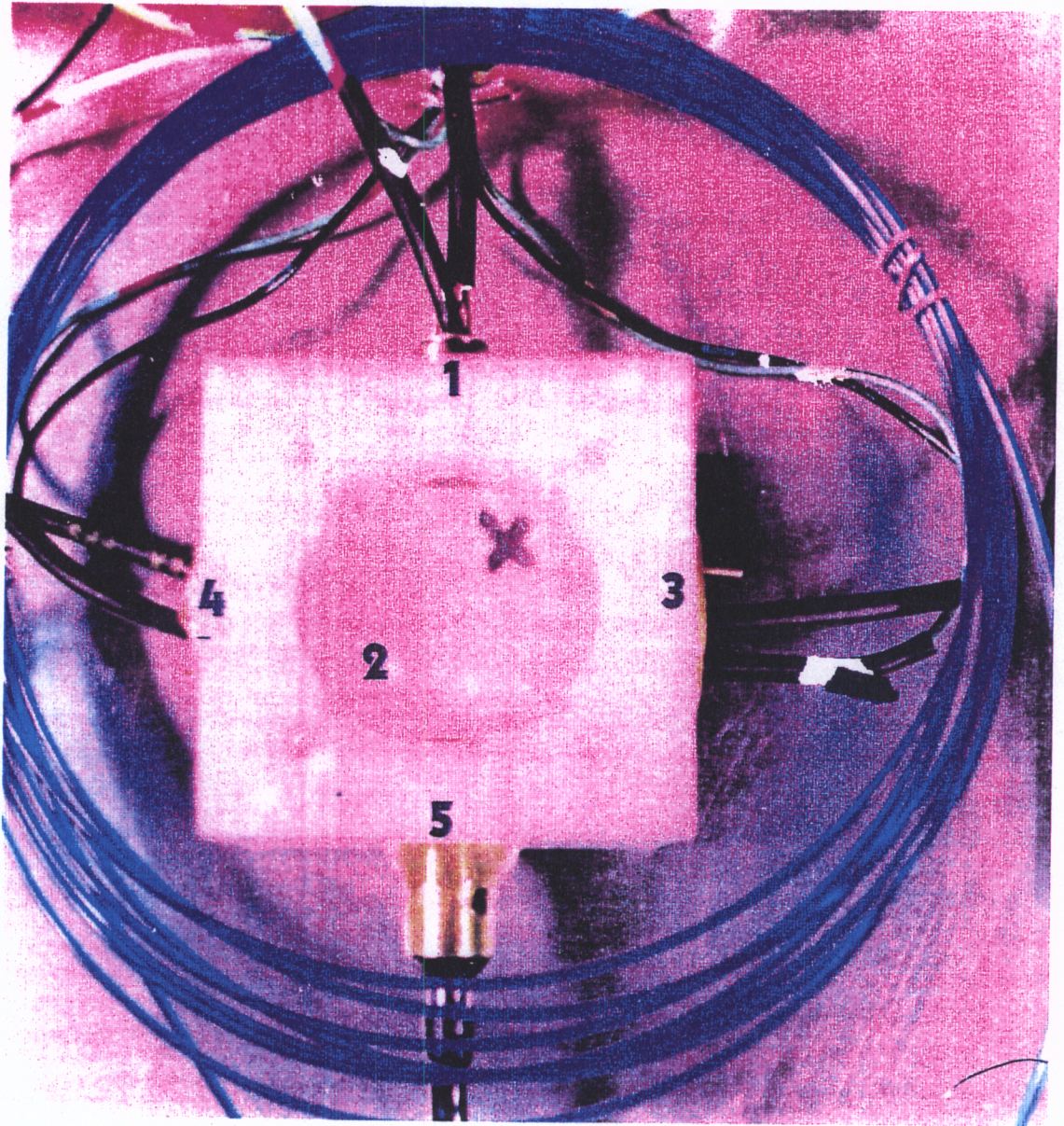


Figure 23. The source/detector system with the LED/lens barrel and the fiber/lens barrel.

coupler multimode fiber are excited compared to the injecting multimode fiber. Figure 25 shows the graph of modal power distribution of a particular system. The Gaussian shaped plot of the modal power distribution indicates that all the modes of the fiber have been excited equally.

4.2 Coupler Tapering Stage

The coupler tapering stage has two positioners on which the fibers can be fixed and twisted. These positioners are controlled by a DC motor. The function of the DC motor is to pull the stages apart tapering the bundle of fibers after they are heated. The coupler tapering stage is shown in Figure 26.

4.3 Software

A computer is used to acquire data, with the help of two data acquisition cards, DT2801™ and DT2814™, from the detectors. The software controls the switching of LEDs so that only one LED is on at any instant of time and also selects the detectors to be sampled. The software has five subroutines listed below, which have to be executed before making the coupler.

i) Direction of Coupling

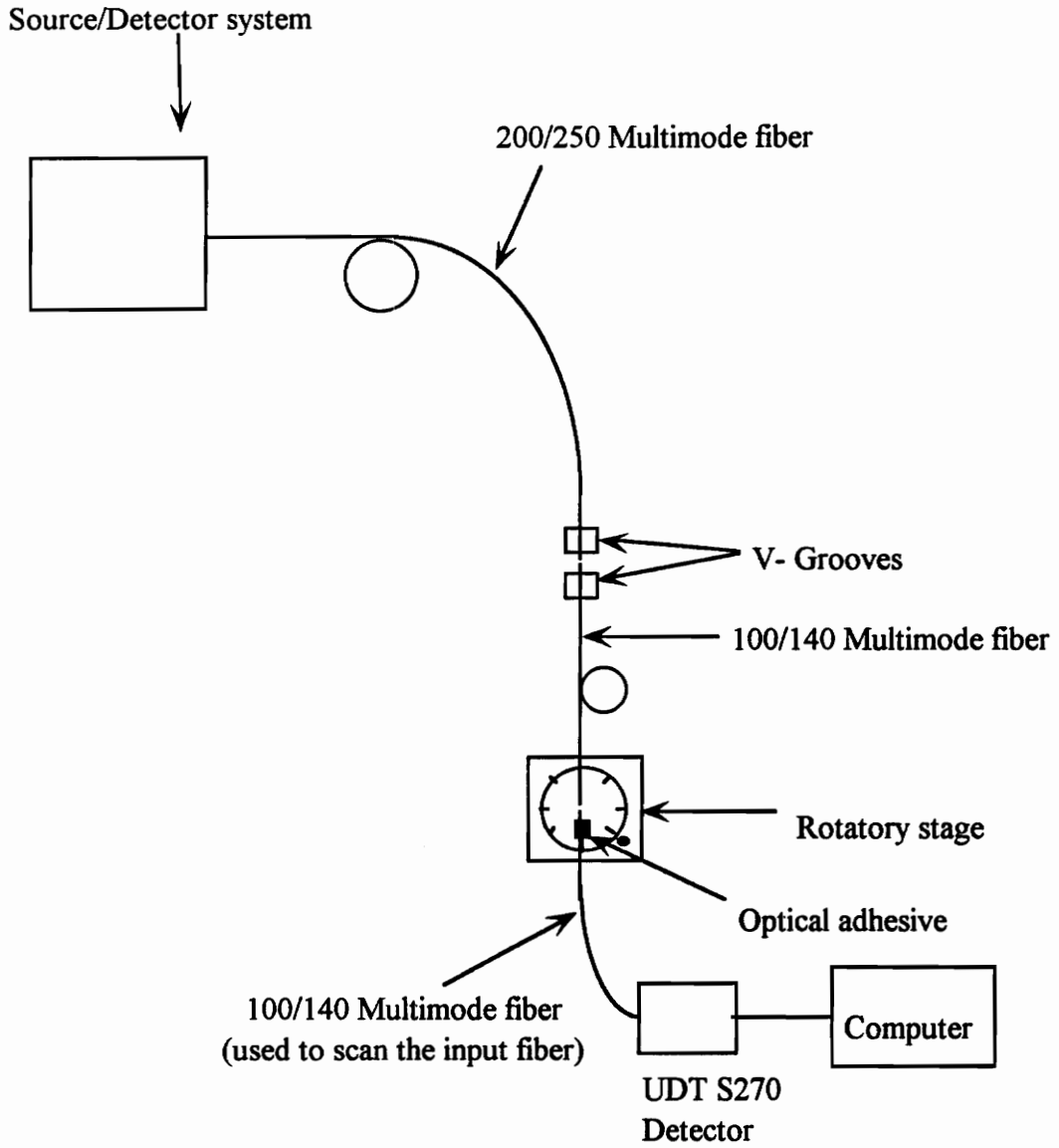


Figure 24. Experimental setup for measuring modal power distribution of the fibers.

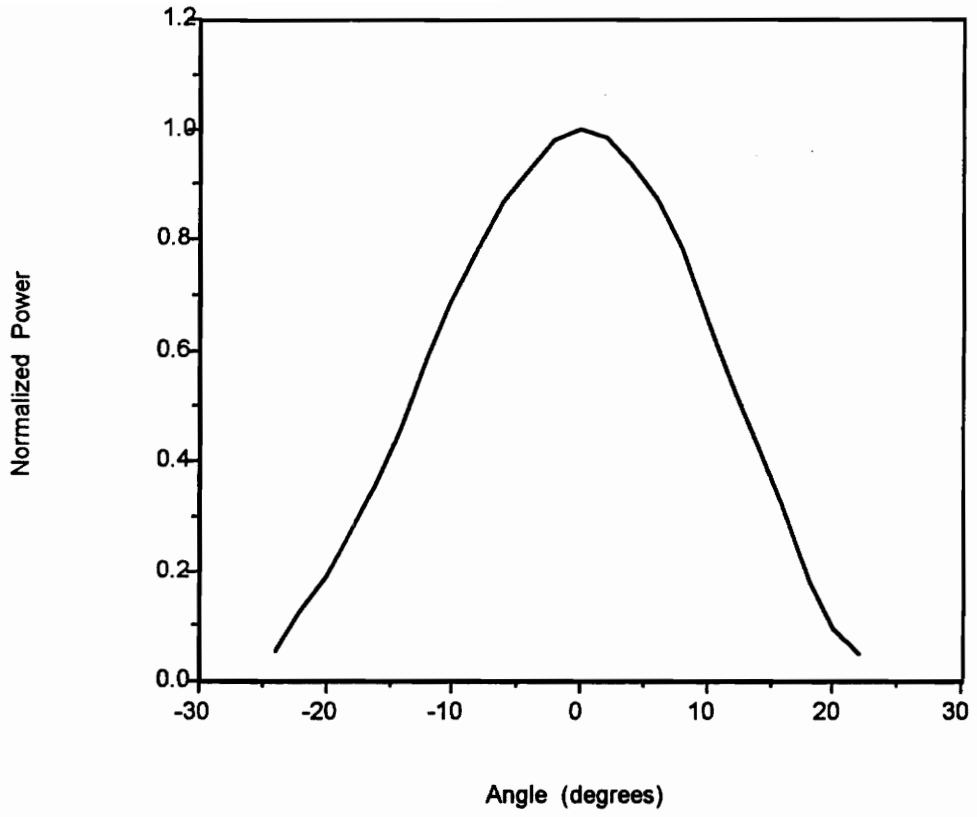


Figure 25. Plot of modal power distribution for unit #6.

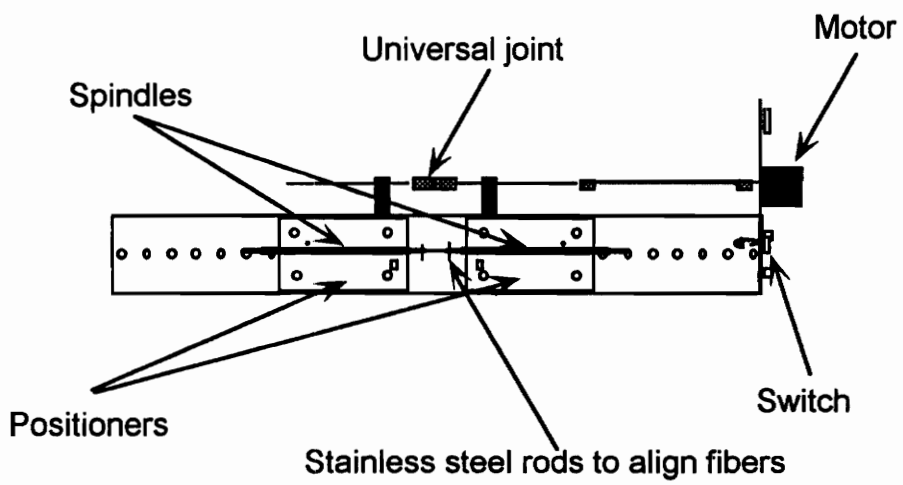


Figure 26. Coupler tapering stage.

The direction of the coupling will have to be chosen to be left or right, since the coupler station is capable of making bi-directional measurements on the coupler. The units of the coupler station are numbered 1 through 16, units 1 through 9 make up the left side of the system and units 9 through 16 comprise of the right side of the system. When the direction of coupling is chosen to be left side source/detector arrays 1 through 9 act as the sources, while source/detector arrays 9 through 16 act as the detectors.

The photodiode dark current is the current that continues to flow through the bias circuit of the device when no light is incident on the photodetector. The dark current arises from the electrons and/or holes which are thermally generated in the pn junction of the photodiode. The measurements made on the coupler will not be accurate if the dark currents are not taken into account. The errors due to the dark currents can be eliminated by measuring them and subtracting from the measured power reading. The dark currents of all the detectors are measured and stored in a look-up table for reference and compensation each time a measurement is taken.

ii) Normalization

The detectors of the sixteen units have to be normalized. This is done by switching on a common LED and taking power measurements on the throughput side of the fiber at all detectors. All the detectors in the system are normalized with respect to the lowest reading. These factors are stored in an array and are accessed every time a measurement is taken. When a throughput voltage is measured, the measured voltage is multiplied by

the normalization factor to obtain a correct reading. The reason for doing normalization is to make sure that the voltage recorded by the computer reflect variations due to the coupler and not due to different sources and detectors.

iii) Throughput Measurements

The fibers are placed in the v-grooves in between the corresponding units for e.g. 1 is connected to 9 etc. A direction of coupling is chosen and each LED is turned on and the output of the fiber at the respective detectors is measured in terms of voltage. The direction of coupling is changed and the throughputs for the fiber on the other side are measured and recorded. The throughput power is recorded as voltage in a lookup table. These throughputs are used to calculate the parameters of the coupler once it is made.

Once all the preliminary steps are completed, one of the LEDs is turned on and the fibers are fused and tapered. A dynamic display of the power coupled into ports during fusion of the coupler is displayed. The power coupled into each port obtained from the following equation is displayed in dBs.

$$P_{ij} = 10 \log \left(\frac{VC_j}{VT_i} \right), \quad (4.2)$$

where VC_j is voltage measured at detector of port j after coupler is made,

VT_i is the throughput voltage measured with port i as the injecting port,

and P_{ij} is the power coupled into port j with port i acting as the injecting port.

The input power is monitored by the reference detector and if there is a fluctuation of >2% in the source the software updates the throughputs by the same amount. After the fusing is complete the remaining LEDs are turned on sequentially, output power at each port is recorded. Power coupled into the ports due to fusion is calculated and displayed. A matrix is built displaying the input ports and the corresponding output powers. An example of the table is shown below in Figure 27. The uniformity and the insertion loss are calculated and displayed.

| LED No. / Channel | COUPLER NUMBER 1 | | | | | | | |
|-------------------|------------------|-------|-------|-------|-------|-------|-------|-------|
| | 1 | 2 | 3 | 4 | 5 | 6 | 7 | 8 |
| 9 | -8.9 | -9.9 | -10.6 | -10.4 | -10.4 | -10.7 | -10.5 | -10.1 |
| 10 | -11.4 | -8.0 | -11.3 | -11.2 | -11.1 | -11.2 | -11.1 | -10.8 |
| 11 | -10.7 | -9.9 | -8.3 | -10.5 | -10.6 | -10.6 | -10.5 | -10.2 |
| 12 | -11.1 | -10.3 | -10.9 | -8.7 | -10.8 | -10.8 | -10.7 | -10.5 |
| 13 | -10.9 | -10.0 | -10.9 | -10.7 | -8.1 | -10.8 | -10.7 | -10.2 |
| 14 | -10.7 | -9.9 | -10.7 | -10.5 | -10.4 | -8.8 | -10.6 | -10.1 |
| 15 | -10.9 | -10.2 | -11.0 | -10.7 | -10.8 | -10.9 | -8.4 | -10.4 |
| 16 | -11.1 | -10.5 | -11.2 | -10.9 | -10.9 | -11.2 | -11.0 | -8.1 |

Uniformity = 3.4dB Insertion loss= -8.0dB All values in dB
 Hit <shift> <Print Screen> to print array
 Enter B/b to return to main menu?

Figure 27. Transmission matrix produced by the software.

5.0 Results

This chapter discusses the experimental setup and results of the tests conducted. The first section presents the results obtained by performing the push-pull modification technique and are compared to the data obtained by performing the diffusion technique, on 8x8 multimode couplers to improve uniformity. The results of several diffusion tests performed are presented in Section 5.2 and the tradeoff between the excess loss and uniformity with diffusion is demonstrated.

5.1 Push-Pull Technique

Multimode fiber with 100/140 core/cladding diameter micrometers was used to manufacture the couplers. The fiber has a germanium doped core and an undoped cladding. Couplers were manufactured by the push and pull technique to obtain data for comparison. The method of manufacture of couplers by this technique is shown in Figure 28. Fibers are first stripped in the center, cleaned and loaded onto the coupler tapering

stage. The ports of the coupler are placed in the corresponding v-grooves and throughputs are recorded. The fibers are heated and tapered with the help of an oxy-propane torch till a reasonable uniformity is achieved. Table I shows the transmission matrix recorded by the computer, and as can be seen from the table the uniformity for the coupler is very high. The tapering is stopped and the push pull technique is applied, and Table II shows the transmission matrix for the coupler. The uniformity of the coupler is improved from 3.5dB to 1.1dB by the push-pull technique.

5.2 Diffusion Technique

The diffusion techniques were attempted on couplers made out of two different fibers each having a different core/cladding ratio. The 62.5/125 micrometer core/cladding fiber has a core/cladding ratio of 0.5 and the 100/140 micrometer core/cladding fiber has a core/cladding ratio of 0.7.

5.2.1 Results of 100/140 Multimode Fiber Couplers

All experimental data presented for the 100/140 micrometer core/cladding diameter multimode fibers is for 8x8 couplers. The fibers are first stripped in the middle, cleaned and loaded onto a coupler manufacturing station developed by us. The fiber bundle is then fused at temperatures from about 1500°C-1700°C and tapered. The transmission matrix of the coupler at this point is shown in Table III. Tapering of the coupler reduces the separation of the individual cores in the minimum taper region allowing for coupling to take place. As can be seen from Table III the throughput port is always at least 2dB greater than the other ports and uniformity of the coupler is 3.3dB.

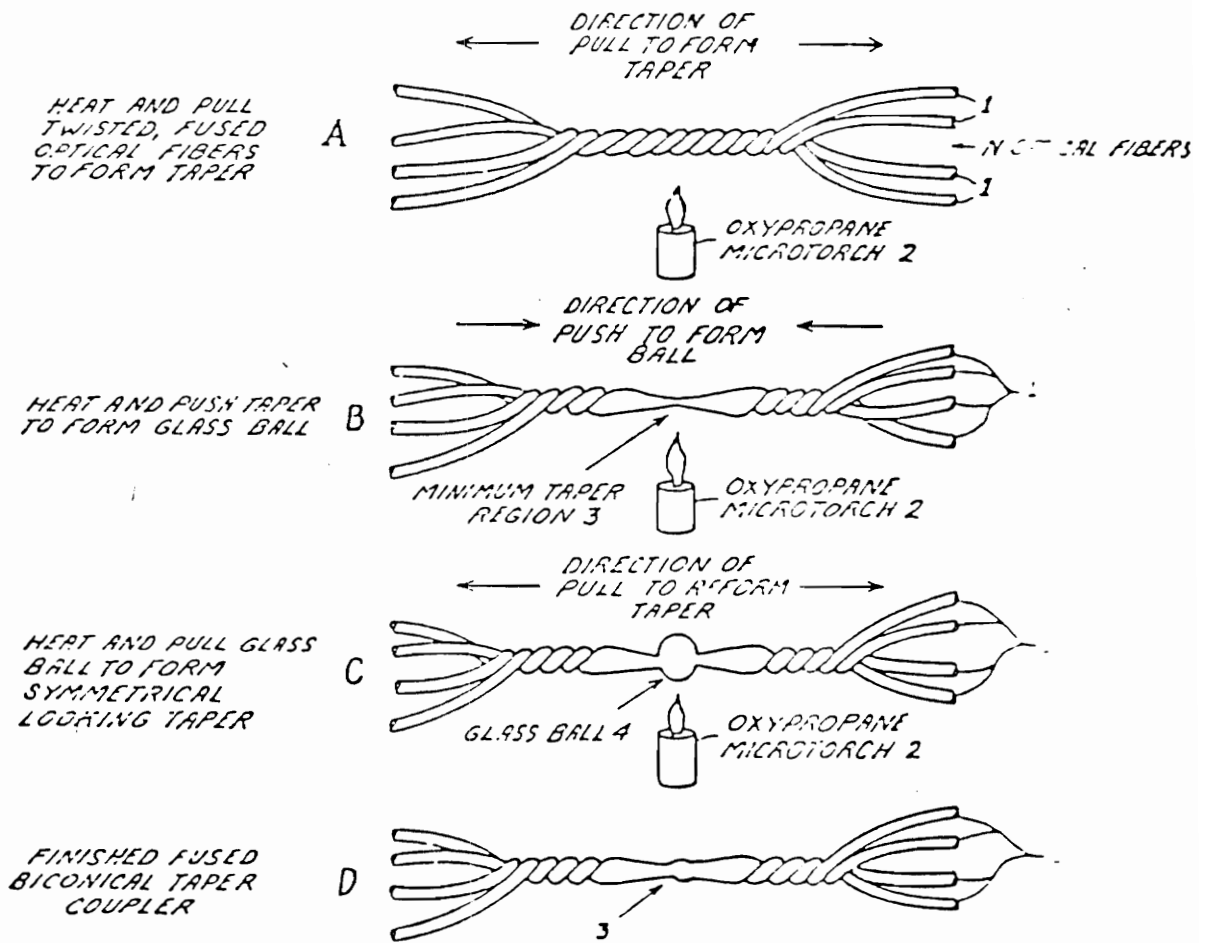


Figure 28. Push-pull method.

Table I. Transmission matrix of the coupler before uniformity improvement

| | | Input Ports | | | | | | | |
|----|--------------|---------------|---------------|--------------|---------------|---------------|---------------|---------------|---------------|
| | | 1 | 2 | 3 | 4 | 17 | 18 | 19 | 20 |
| 17 | Output Ports | - 11.1 | - 14.4 | - 13.2 | - 14.4 | | | | |
| 18 | | - 14.2 | - 11.0 | - 12.8 | - 13.9 | | | | |
| 19 | | - 14.9 | - 14.5 | - 9.9 | - 14.4 | | | | |
| 20 | | - 14.1 | - 13.8 | - 12.5 | - 11.5 | | | | |
| 1 | | | | | | - 11.3 | - 14.6 | - 13.4 | - 14.2 |
| 2 | | | | | | - 13.9 | - 10.1 | - 12.5 | - 13.3 |
| 3 | | | | | | - 15.0 | - 14.8 | - 11.1 | - 14.3 |
| 4 | | | | | | - 14.0 | - 13.8 | - 12.5 | - 10.8 |

All values in dB

Uniformity = 5 dB

Table II. Transmission matrix of the coupler after push-pull technique is applied

| | | Input Ports | | | | | | | |
|----|-------|--------------|--------------|--------------|--------------|--------------|--------------|--------------|----|
| | | 1 | 2 | 3 | 4 | 17 | 18 | 19 | 20 |
| 17 | -14.7 | -14.6 | -13.4 | -14.8 | | | | | |
| 18 | -14.5 | -14.0 | -13.0 | -14.3 | | | | | |
| 19 | -15.1 | -14.9 | -13.3 | -14.5 | | | | | |
| 20 | -14.4 | -14.1 | -12.9 | -14.1 | | | | | |
| 1 | | | | | -14.8 | -14.8 | -13.7 | -14.6 | |
| 2 | | | | | -14.1 | -13.6 | -12.8 | -13.6 | |
| 3 | | | | | -15.3 | -15.1 | -13.8 | -14.8 | |
| 4 | | | | | -14.3 | -14.3 | -12.5 | -13.7 | |

All values in dB

Uniformity = 2.5 dB

Table III. Transmission matrix of the coupler before uniformity improvement technique.

| | | Input Ports | | | | | | | |
|----|--|-------------|-------|-------|-------|-------|-------|-------|-------|
| | | 1 | 2 | 3 | 4 | 5 | 6 | 7 | 8 |
| 9 | | -8.7 | -9.7 | -10.5 | -10.1 | -10.3 | -10.4 | -10.3 | -9.9 |
| 10 | | -11.1 | -7.8 | -11.1 | -10.9 | -11 | -11 | -11 | -10.6 |
| 11 | | -10.6 | -9.8 | -8.2 | -10.2 | -10.5 | -10.4 | -10.4 | -10 |
| 12 | | -10.9 | -10.1 | -10.8 | -8.4 | -10.7 | -10.6 | -10.6 | -10.3 |
| 13 | | -10.6 | -9.9 | -10.8 | -10.3 | -8.1 | -10.6 | -10.5 | -10 |
| 14 | | -10.6 | -9.8 | -10.6 | -10.2 | -10.4 | -8.6 | -10.4 | -10 |
| 15 | | -10.8 | -10 | -10.9 | -10.4 | -10.7 | -10.7 | -8.3 | -10.2 |
| 16 | | -11.1 | -10.3 | -11.1 | -10.7 | -10.8 | -11 | -10.8 | -8 |

All Values are in dB

The minimum taper region is then diffused at a temperature of about 1300°C to improve the uniformity of the coupler. Diffusion in this case results in the migration of the germanium dopants into the cladding resulting in an increase in the effective size of the core and at the same decreasing the refractive index of the core. Diffusion thus helps in reducing the separation of the cores enabling uniform power transfer into the other cores. Table IV shown below shows the transmission matrix of the coupler after diffusion, and the uniformity of the coupler after diffusion is 1.8dB. Table V shows the improvement of uniformity of the coupler, with port 1 acting as the injecting port, at various times for another coupler. Table VI summarizes the results of diffusion tests on 8x8 couplers.

As can be seen from Table VI there has been a noticeable improvement in the uniformity of all the couplers but this improvement has invariably been accompanied by an increase in excess loss. C.W.Pickett et al. [24] related the losses in singlemode couplers to dopant diffusion. Krause et al.[23] related splice loss of single mode fiber to diffusion. A similar phenomenon is noticed in multi-mode couplers and as a result of diffusion the excess loss of the coupler also increases. Figure 29 shows the tradeoff between excess loss and uniformity with time and the optimal point at which diffusion can be stopped for the coupler diffused at 1350°C.

Figures 30 and 31 show improvement in uniformity, and increase in excess loss of couplers diffused at various temperatures respectively. It can be seen from Figure 31 that uniformity improvement occurs faster at higher temperatures, because the dopant transportation increases with an increase in temperature. The uniformity for a coupler diffused at 1500° C decreased from 3 dB to 0.6 dB in 2 minutes. The uniformity for a coupler diffused at 1300° C decreased from 2.5 dB to 1.4 dB in about 12 minutes. The

uniformity for a coupler diffused at 1100° C decreased from 3.2 dB to 1.35 dB in 32 mins. Diffusion of the coupler at high temperatures is accompanied by a rapid increase in the excess loss of the coupler. The excess loss for a coupler diffused at 1500° C, 1300° C, 1100° C increased by 0.6 dB, 0.5 dB and 0.9 dB respectively. Couplers thus have to be diffused at temperatures that will result in better uniformity , low excess loss and at the same time be manufactured within a reasonable time so as to get a high yield on the process. It can be seen from Figures 31 and 32 that the ideal temperature to perform diffusion on the coupler is 1300° C.

5.2.2 Results of 62.5/125 Multimode Fiber Couplers

Preliminary experimental data presented on 62.5/125 micrometer core/cladding multimode fiber couplers is for 2x2 couplers. The fibers are first stripped in the middle, cleaned and loaded onto a coupler manufacturing station. The fiber bundle is then fused at a temperature of 1500°C-1700°C, and tapered to a length of 0.8 cm and the coupler is then diffused. The transmission matrix of the coupler after tapering and during diffusion is shown in Table VII. It can be seen from the Table VII that the excess loss for the coupler is very high but there is a definite improvement in the uniformity. The transmission matrix of the coupler with a taper length of 0.5 cm. after tapering and during diffusion is shown in Table VIII. Excess Loss for the coupler is 1.6dB.

Modal power distribution of the throughput port before fusion, after fusion and diffusion, and the modal power distribution of the tapoff fiber after fusion and diffusion are shown in Figures 32, 33, 34 respectively. It can be seen from Figures 34 and 35 that the power is being coupled into all modes uniformly for both the throughput fiber and the tapoff fiber.

Table IV. Transmission matrix of the coupler after diffusion technique is applied.

| | | Input Ports | | | | | | | |
|--------------|----|-------------|-------|-------|-------|-------|-------|-------|-------|
| | | 1 | 2 | 3 | 4 | 5 | 6 | 7 | 8 |
| Output Ports | 9 | -9.9 | -9.7 | -10.5 | -10.2 | -10.1 | -10.5 | -10.3 | -9.9 |
| | 10 | -11.2 | -9.9 | -10.9 | -10.8 | -10.6 | -10.6 | -10.9 | -10.5 |
| | 11 | -10.7 | -9.7 | -10.1 | -10.2 | -10.1 | -10.3 | -10.4 | -10 |
| | 12 | -11 | -10 | -10.7 | -10.1 | -10.4 | -10.7 | -10.6 | -10.2 |
| | 13 | -10.8 | -9.8 | -10.7 | -10.4 | -9.6 | -10.6 | -10.6 | -10.1 |
| | 14 | -10.7 | -9.5 | -10.4 | -10.3 | -10.1 | -10 | -10.4 | -10 |
| | 15 | -11 | -10.1 | -10.9 | -10.6 | -10.5 | -10.9 | -9.7 | -10.3 |
| | 16 | -11.1 | -10.3 | -11 | -10.8 | -10.6 | -11 | -10.9 | -9.4 |

All Values are in dB

Table V. Improvement in uniformity of the coupler with time.

| | | Time | | |
|--------------|------------|-------|---------|---------|
| | | 0 sec | 325 sec | 405 sec |
| Output Ports | 9 | -8.7 | -9.4 | -9.9 |
| | 10 | -11.1 | -10.8 | -11.2 |
| | 11 | -10.6 | -10.2 | -10.7 |
| | 12 | -10.9 | -10.6 | -11 |
| | 13 | -10.6 | -10.4 | -10.8 |
| | 14 | -10.6 | -10.4 | -10.7 |
| | 15 | -10.8 | -10.5 | -11 |
| | 16 | -11.1 | -10.7 | -11.1 |
| | Uniformity | -2.4 | -1.3 | -1.2 |

Injection Port
#1

All values in dB

Temp. 1350°C

Table VI. Results of diffusion tests on 8x8 couplers.

| Coupler# | Before Diffusion | | After Diffusion | |
|----------------|------------------|-------------|-----------------|-------------|
| | Uniformity | EL | Uniformity | EL |
| 1 | 3.3 | 1.45 | 1.8 | 1.75 |
| 2 | 4.2 | 1.21 | 1.77 | 3.5 |
| 3 | 4.5 | 1.08 | 1.95 | 1.91 |
| 4 | 4.12 | 1.57 | 1.6 | 2.71 |
| 5 | 3.54 | 1.18 | 0.86 | 1.96 |
| 6 | 3.01 | 2.05 | 0.6 | 2.65 |
| 7 | 2.47 | 1.34 | 1.34 | 1.98 |
| Average | 3.59 | 1.41 | 1.41 | 2.35 |

All values in dB

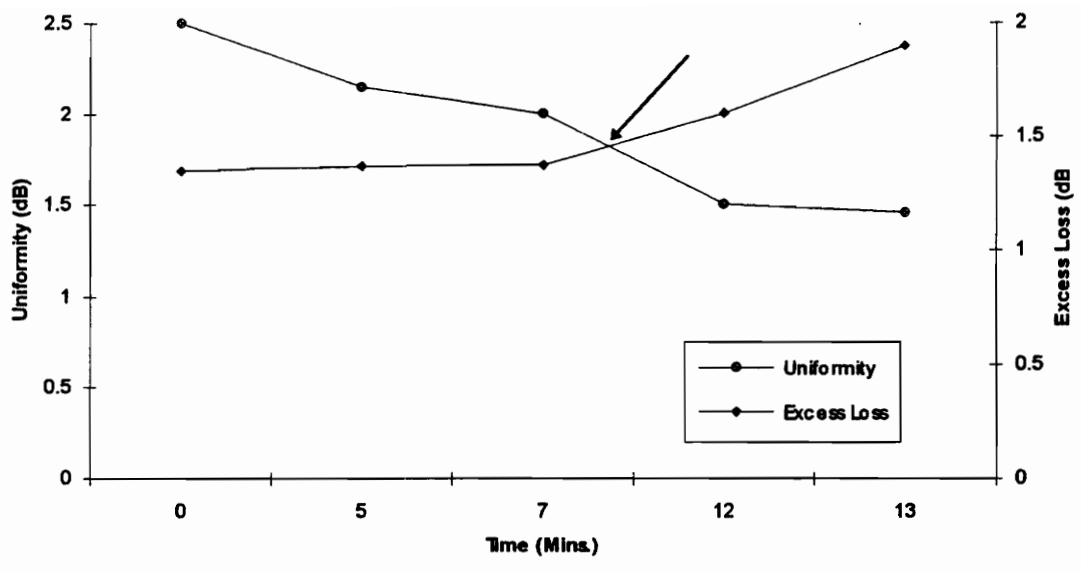


Figure 29. The comparison of tradeoff between excess loss and uniformity with time. The optimal point at which diffusion can be stopped for the coupler diffused at 1350°C.

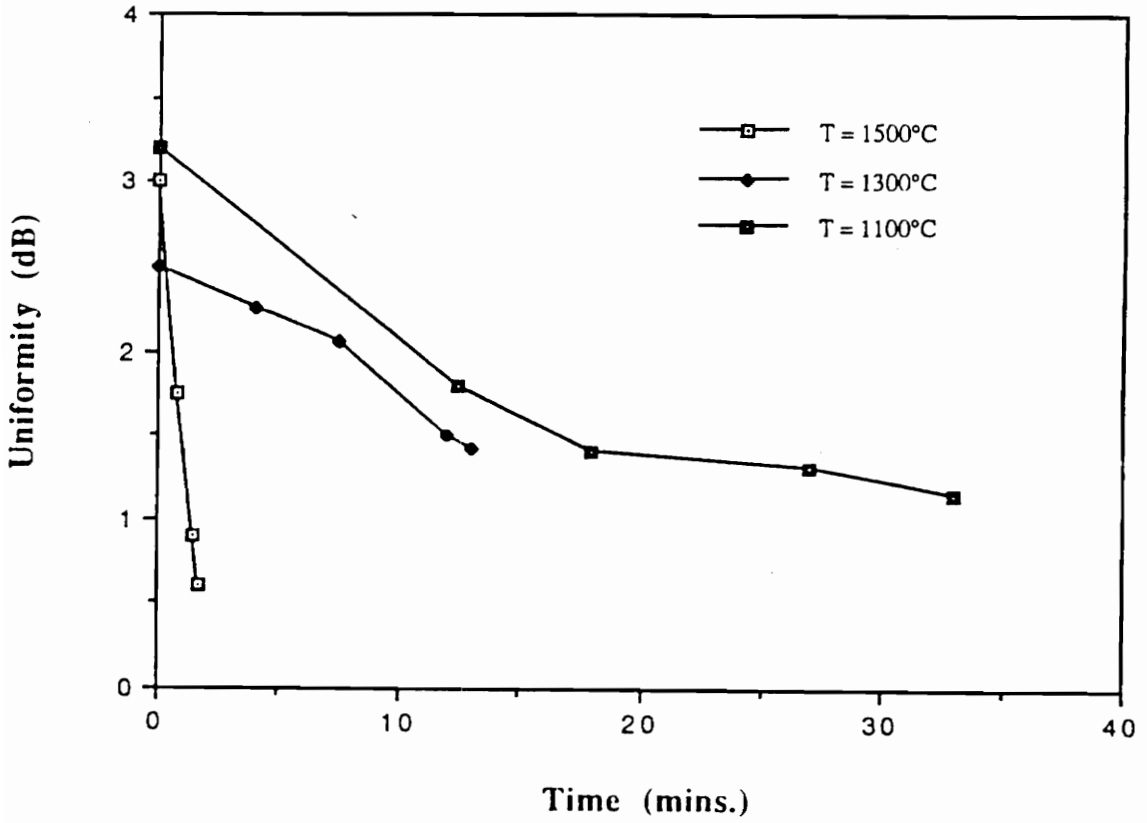


Figure 30. Uniformity versus time at various temperatures.

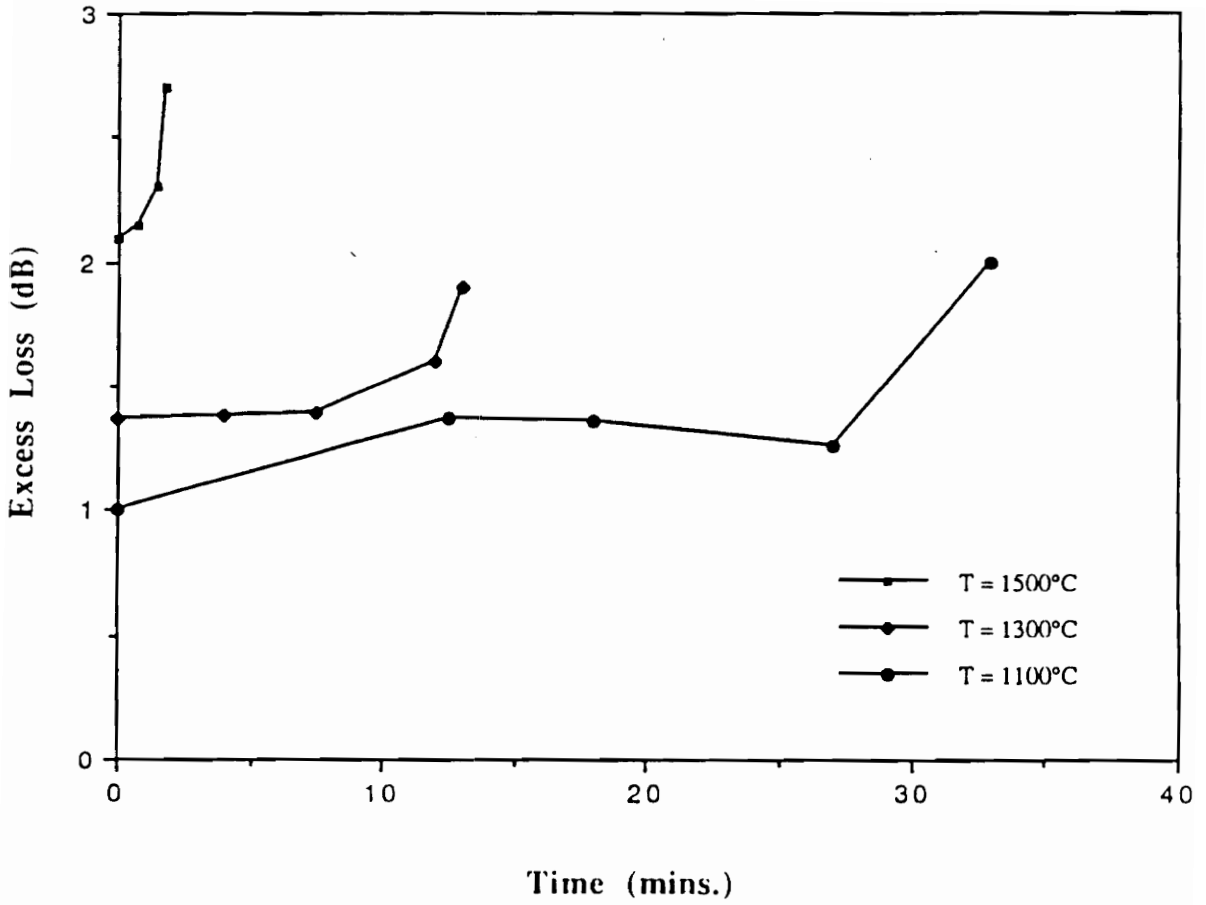


Figure 31. Excess loss versus time at various temperatures.

Table VII. Transmission matrix of coupler with a taper length of 0.8 cm during diffusion.

Taper Length = 0.8 cm

| Diffusion Time(Sec) | Port1 | Port2 |
|---------------------|-------|-------|
| 0 | 1.07 | 8.26 |
| 30 | 2.8 | 5.91 |
| 60 | 2.87 | 5.69 |
| 90 | 3.18 | 5.15 |
| 110 | 3.89 | 4.34 |
| 130 | 4.1 | 4.15 |

Table VIII. Transmission matrix of coupler with a taper length of 0.5 cm during diffusion

Taper Length = 0.5 cm

| Diffusion Time(Sec) | Port1 | Port2 |
|---------------------|-------|-------|
| 0 | -9.4 | -1.9 |
| 15 | -7.6 | -2.3 |
| 30 | -7.3 | -2.4 |
| 92 | -7.2 | -2.8 |
| 117 | -6.67 | -3.1 |
| 137 | -6.5 | -3.2 |
| 162 | -5.7 | -3.5 |
| 182 | -4.5 | -4.7 |

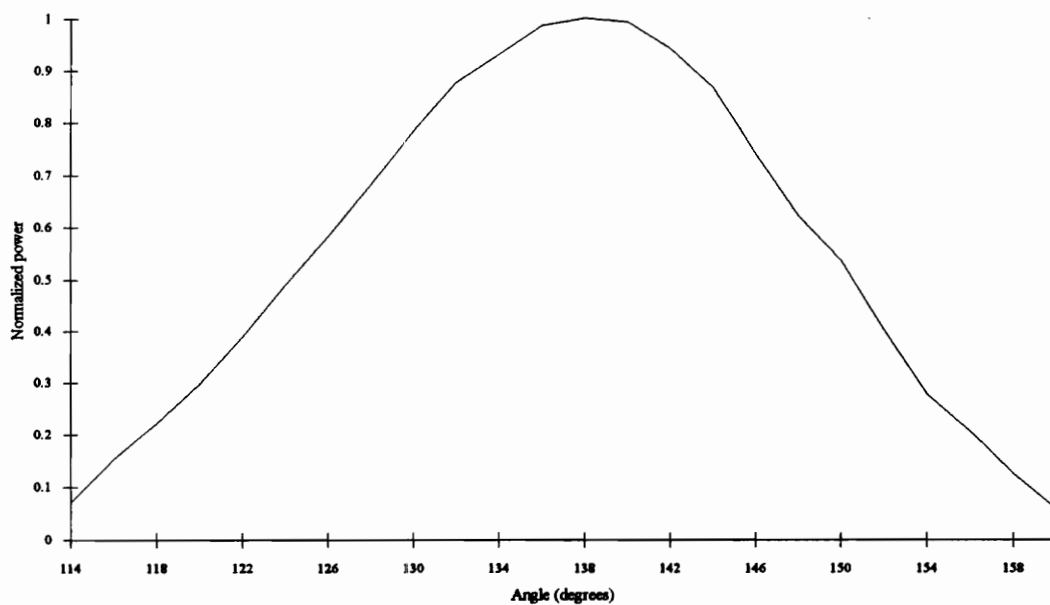


Figure 32. Modal power distribution of throughput fiber before fusion.

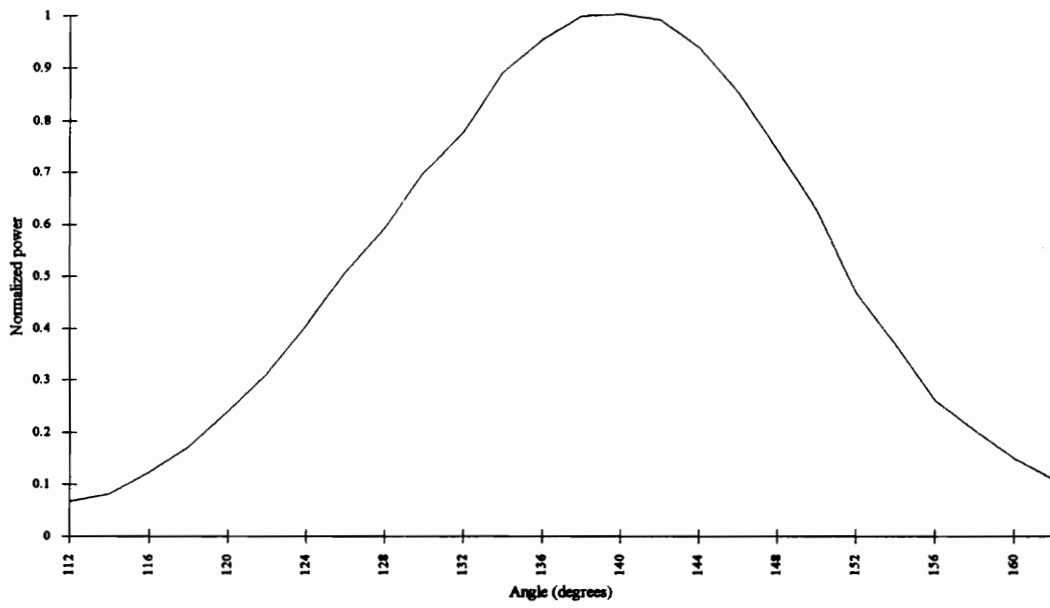


Figure 33. Modal power distribution of throughput fiber after diffusion.

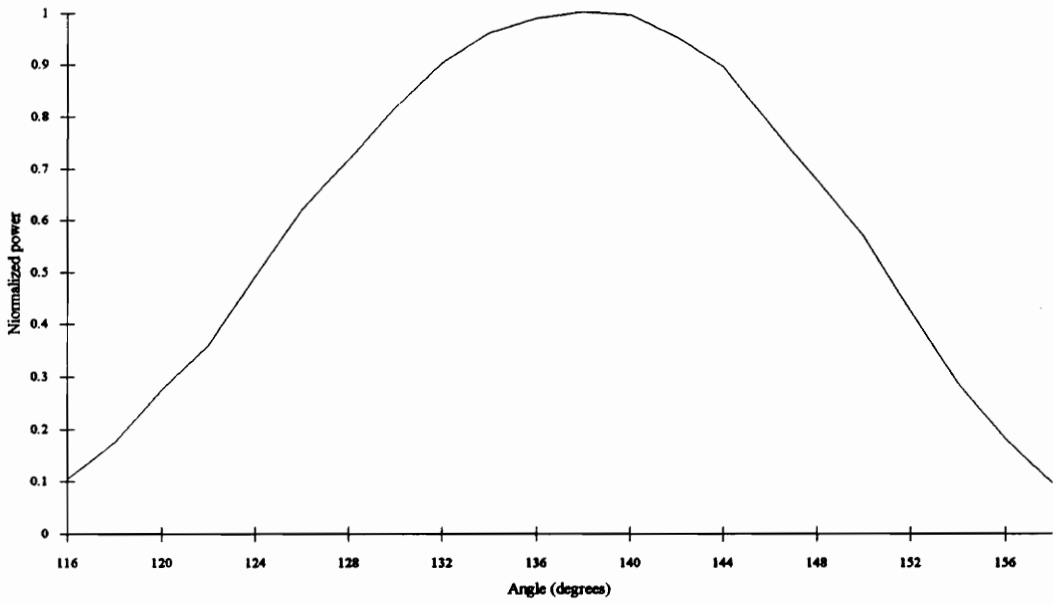


Figure 34. Modal power distribution of tapoff fiber after diffusion.

6.0 Conclusions

A coupler measurement station, which simplifies the process of coupler manufacturing and greatly reduces the time taken for manufacturing a coupler, has been developed, fabricated and tested. The measurement station is capable of making bi-directional measurements and gives the user the capability of dynamically monitoring the output ports of the coupler during the process of manufacturing of the coupler.

It also has been shown that diffusion of dopants in the minimum taper region of the coupler improves the uniformity among the coupler ports. This technique can be employed to improve uniformity of multimode couplers irrespective of the core/cladding ratio. However, improvement in uniformity is accompanied by an increase in the excess loss of the coupler. The amount of diffusion the coupler is subjected to is thus a tradeoff between improvement in uniformity and increase in excess loss. It is also dependent on the temperature at which the coupler is diffused. The ideal temperature for diffusion,

which will yield couplers that meet the specifications of uniformity and excess loss has been identified. The preliminary results of 62.5/125 micrometers diameter core, cladding multimode fiber couplers are very promising. The excess loss of the couplers can be decreased with controlled thermal diffusion of the dopants. Manufacturing 62.5/125 micrometers diameter core, cladding multimode fiber couplers by diffusion process will do away with the messy process of etching the cladding.

The diffusion technique presented in this thesis has its advantages when compared to the other techniques of uniformity improvement. This technique lowers the skill level of the operator required to manufacture couplers. Diffusion technique further introduces the possibility of developing automated systems to manufacture multimode couplers with low excess loss and good uniformity.

Future work could include complete automation of the coupler station by automating the fusion process. This can be achieved by replacing the oxy-propane torch with a mini high temperature furnace. Another step towards complete automation would be controlling the speed of the motor that tapers the coupler and controlling the temperature of the furnace by software. The excess loss and uniformity could be tracked to determine the optimum point at which diffusion can be terminated. The use of a furnace instead of an oxy-propane torch for diffusion will give better control over thermal diffusion and definitely yield couplers with low excess loss and better uniformity.

Future work could also include more experiments on low core/cladding ratio fiber couplers. Another method of manufacture that could be investigated is diffusion of individual fibers without tapering so that the core/cladding ratio decreases and manufacturing the coupler. Work has been done in expanding the core size of singlemode fibers by subjecting them to thermal diffusion [25-29].

7.0 References

- [1] N.L. Rhodes, "Interacting a network design and fiber optic components design in LANs", *IEEE J. Selected Areas of Communication*, vol. SAC-1, pp. 489, 1983.
- [2] J.Sasaki, S.Suzuki, "Fiber optic star-ring LAN using optical couplers", *Proc. of FOC/LAN*, 1988, pp. 241-246.
- [3] S.D. Personick, "Application of fiber optics in LAN", *Proc. 8th European Conference Optical Fibers*, Sept. 1982, pp. 425.
- [4] D.C. Johnson, B.S. Kawasaki, and K.O. Hill, "Fused biconical tapered fiber-optic devices: Application to data buses", *Fiber and Integrated Optics*, vol. 3, no. 2-3.

- [5] Ozan. K. Tonguz, "Fiber optic interconnection of local area networks: physical limitations of topologies", *Journal of Lightwave Tech.*, vol. 11, no. 5/6, May/June 1993.
- [6] R. Griffin, J.D. Love, P.R.A. Lyons, D.A. Thorncraft, and S.C. Rashleigh, "Assymetric multimode couplers", *Journal of Lightwave Tech.*, vol. 9, no.11, November 1991.
- [7] Schelto van Doorn, "Fiber optic couplers", SPIE vol. 574, *Fiber optic couplers, connectors and splice technology, II* (1985).
- [8] Shigeo Matsushita, Kawai, and Hisahi Uchida, "Fiber optic devices for LAN applications", *Journal of Lightwave Technology*, Vol. LT-3 No. 3, June 1985, pp 544-556.
- [9] E. G. Rawson, and M. D. Bailey, "Bitaper star couplers with upto 100 fiber channels", *Electron Lett.*, Vol.15, pp 432-433, 1979.
- [10] Shigeru Ohshima, Takao Ito, Ken-Ichi Donuma, Hisayoshi Sugiyama and Yohji Fujii, "Small loss-deviation tapered fiber star coupler for LAN", *Journal of Lightwave Technology*, Vol. LT-3, No. 3, June 1985, pp 556-560.
- [11] Piet J. Severin, Ad D. Severijns, and Cor H van Bommel, "Passive components for multimode fiber optic networks", *Journal of Lightwave Technology*, Vol. LT-4, No. 5, May 1986, pp 490-496.
- [12] L. J. Coyne, "Distributed fiber optic couplers using rectangular light guides as mixing elements" in *Proc. Fiber Optics and Commn.*, 1977, pp 160-164.

- [13] Kent A. Murphy, "Method of Fabricating a Low Loss Fused Biconical Tapered Fiber Optic Coupler", *U.S. Patent 4,426,215*, 1983.
- [14] Kent A. Murphy, "Method of Fabricating a Low Loss Fused Biconical Tapered Fiber Optic Coupler",
- [15] Gerd Keiser, *Optical Fiber Communications*, McGraw-Hill, New York, 2nd ed., 1991.
- [16] M. J. Adams, *An Introduction to Optical Waveguide Theory*, Mc-Graw Hill, New York, 1981.
- [17] D. Krumbholz, E. Brinkmeyer, and E.G, Neumann, "Core/Cladding power distribution, propagation constant, and group delay; Simpler relation for power law graded-index fibers", *Journal of Optical Society of America*, Vol. 70, No. 2, Feb. 1980, pp 179-183.
- [18] D. Gloge, E. A. J. Marcatili, "Impulse response of fibers with ring-shaped parabolic index distribution", *Bell Systems Technical Journal*, Sept. 1973, pp 1161-1168.
- [19] D. Gloge, "Weakly guiding fibers", *Applied Optics*, Vol. 10, No. 10 , Oct. 1971, pp 2252-2258.
- [20] J.S. Harper, C.P. Botham, and S. Hornung, "Theory of tapering singlemode optical fibers by controlled core diffusion.", *Electronics Letters*, vol. 24, no. 4, February 1988, pp. 243-245.

- [21] J.S. Harper, C.P. Botham, and S. Hornung, "Tapers in singlemode optical fiber by controlled core diffusion", *Electronics Letters*, vol. 24, no. 4, February 1988, pp. 245-246.
- [22] John T. Krause, W. A. Reed, and K. L. Walker, "Splice loss of single-mode fiber as related to fusion time, temperature, and index profile alteration", *Journal of Light Wave Technology*, Vol. LT-4, No. 7, July 1986, pp 837-840.
- [23] M. N. McLandrich, "Core dopant profiles in weakly guiding fused single-mode fibers", *Electronics Letters*, Vol. 24, No. 1-13, 1988, pp 8-10.
- [24] C. W. Pickett, W. K. Burns, and C. A. Villarruel, "Dopant diffusion loss mechanism in high-birefringent-fiber fused couplers", *Optics Letters*, Vol. 13, No. 10, pp 835-837.
- [25] Kazuo Shiraishi, Yoshizo Aizawa, and Shojiro Kawakami, "beam expanding fiber using thermal diffusion of dopant", *Journal of Light Wave Technology*, Vol. LT-8, No. 8, August 1990, pp 1151-1161.
- [26] H. hanafusa, M. Horiguchi, and J. Noda, "Thermally diffused expanded core fibers for low loss and inexpensive photonic components", *Electronics Letters*, vol. 4, 1992, p. 465
- [27] M. Kihara, S. Tomita, and M. Matsumoto, "Loss characteristics of thermally diffused expanded core fiber", *Photon. tech. Lett.*, vol. 4, 1992, p1390.
- [28] K. Shigihara, K. Shirashi, and S. Kawakami, "Modal field transforming fiber between dissimilar waveguides", *J. Appl. Phys.*, vol. 60, 1986, p. 4293.

- [29] J.S. Harper, C.P. Botham, and S. Hornung, "Tapers in single mode optical fiber by controlled core diffusion", *Electron. Lett.*, vol. 24, 1988, p. 245
- [30] K. Shiraishi, T. Yanagi, Y. Aizawa, and S. Kawakami, "Fiber embedded in-line isolators", *Journal of Light Wave Technology*, Vol. LT-9, 1991, pp 1991.
- [31] J. Stone, L.W. Stulz, C.A. Burrus, and J.C. Centanni, "Fiend filters: Etalon on beveled facet of a fiber with an out-diffused core", *Photon. Tech. Lett.*, vol. 3., 1991, p.216.
- [32] T. Chuzenji, K. Shiraishi, and S. Kawakami, " Lens-free direct integration of optical isolators into a fiber array", *Tech. Dig., Conf. of Opt. Fib. Comm./Int. Conf. on Opt. Fib. Commun.* (San Jose), Feb. 1993.

Vita

The author was born in Madras, India on 16th May 1970, where he resided for two years with his grandparents. He then moved with his parents to Hyderabad, India. He enrolled in Hyderabad Public School, Begumpet, in June 1975 and graduated from that school in May 1987. In the fall of 1987 he entered Chaitanya Bharathi Institute of Technology (affiliated to Osmania University) as an Engineering student. He graduated with a Bachelors Degree in Electrical Engineering in July 1991 from Osmania University. Seeking further knowledge he joined the Graduate Program at Virginia Tech in the Fall of 1991, where the author worked as a graduate research assistant in the Fiber and Electro-Optics Research Center.

